Article

Fasting boosts breast cancer therapy efficacy via glucocorticoid activation

https://doi.org/10.1038/s41586-025-09869-0

Received: 29 February 2024

Accepted: 5 November 2025

Published online: 10 December 2025

Open access

Check for updates

Nuno Padrão[1,2], Tesa M. Severson[1,2], Sebastian Gregoricchio[1,2], Ana Guijarro[3], Catrin Lutz[2,4], Daniel Taranto[2,5], Stefan Hutten[2,4], Francesca Ligorio[6,7], Angelica Persia[3,8], Merel Roest[1,2], Joyce Sanders[9], Ji-Ying Song[10], Sara Pires-Oliveira[9], Maria Donaldson Collier[1,2], Hugo Horlings[9], Livia Pisciotta[3,8], Filippo de Braud[6,11], Claudio Vernieri[7,11], Leila Akkari[2,5], Jos Jonkers[2,4], Alessio Nencioni[3,8], Irene Caffa[3,8]✉ & Wilbert Zwart[1,2,12]✉

The majority of breast cancers are driven by oestrogen receptor-α (ERα) activation, and endocrine therapy represents the mainstay treatment for these patients[1]. However, resistance is common and tumours often progress after years of endocrine suppression[2]. Periodic fasting enhances the efficacy of standard endocrine therapy and delays acquired drug resistance, although the underlying mechanisms remain unclear[3]. Here we show that fasting induces extensive epigenetic reprogramming in ERα-positive breast cancer xenografts when combined with endocrine therapy, with large-scale activation of glucocorticoid receptor (GR) and progesterone receptor signalling and concomitant reduction in the activity of activator protein-1 (AP-1) family members. GR-driven gene programmes are selectively activated in in vivo models of ERα-positive breast cancer during fasting, and GR knockout hinders the anti-tumour effects of fasting combined with tamoxifen. Exogenous administration of GR ligands recapitulates fasting-enhanced anti-oestrogen action, thus promoting tumour regression. Patients undergoing a cyclic fasting-mimicking diet exhibited increased blood progesterone and cortisol concentrations. Additionally, tumours collected after the fasting-mimicking diet showed an inverse correlation of GR activation with proliferation markers, providing clinical confirmation of our observations in animal models. Our results indicate that GR activation has a pivotal role in the ability of fasting to enhance endocrine therapy activity in breast cancer and suggest that corticosteroid administration should be evaluated as an adjuvant to endocrine therapy in this setting.

Hormone receptor-positive (HR^+) breast cancer accounts for 75% of all breast cancer diagnoses, and endocrine therapies represent the mainstay of treatment for patients with HR^+ breast cancer, in both adjuvant and metastatic settings[1]. Yet, the efficacy of standard endocrine therapies is limited by primary or acquired resistance[2]. Periodic fasting enhances the efficacy of endocrine therapies against HR^+ breast cancer and delays acquired therapy resistance in animal models[3]. Clinical studies indicate that cycles of water-only fasting or fasting-mimicking diets (FMDs; low-calorie, low-protein and low-sugar, vegan diets that recreate the metabolic effects of fasting[4]) are feasible and safe in patients with different tumour types, such as breast, melanoma, colorectal, lung and gynaecological cancers[5–7].

We previously reported that fasting enhances the efficacy of endocrine therapies in HR^+ breast cancer[3]. However, the mechanisms that underlie this effect remain unknown. Moreover, adjuvant endocrine regimens involve five to ten years of continuous daily treatment[8], making prolonged combined dietary intervention during endocrine therapy highly challenging to adhere to. Here we investigated the biological mechanisms at the basis of fasting enhancement of tamoxifen (TMX) efficacy, one of the most commonly utilized endocrine therapies, with the aim of identifying therapeutic strategies that phenocopy beneficial effects of fasting or FMD in patients with HR^+ breast cancer, and which could be potentially adopted in place of fasting or FMD.

Fasting reprogrammes the cancer epigenome

In mice xenografted with the human HR^+ breast cancer cell line MCF7, weekly cycles of 48 h fasting showed synergistic in vivo anti-tumour effects when combined with TMX (Fig. 1a,b and Extended Data Fig. 1a,b), confirming our previous observations[3]. To comprehensively define the biological effect of fasting on tumour cell biology, we performed extensive multiomic analyses on the collected tumour material, including transcriptomics, proteomics, immunohistochemistry and chromatin immunoprecipitation with sequencing (ChIP–seq) for

[1]Division of Oncogenomics, The Netherlands Cancer Institute, Amsterdam, The Netherlands. [2]Oncode Institute, Utrecht, The Netherlands. [3]Department of Internal Medicine and Medical Specialties, University of Genoa, Genoa, Italy. [4]Division of Molecular Pathology, The Netherlands Cancer Institute, Amsterdam, The Netherlands. [5]Division of Tumor Biology and Immunology, The Netherlands Cancer Institute, Amsterdam, The Netherlands. [6]Fondazione IRCCS Istituto Nazionale dei Tumori, Milan, Italy. [7]IFOM ETS, the AIRC Institute of Molecular Oncology, Milan, Italy. [8]IRCCS Ospedale Policlinico San Martino, Genoa, Italy. [9]Department of Pathology, The Netherlands Cancer Institute, Amsterdam, The Netherlands. [10]Experimental Animal Pathology, The Netherlands Cancer Institute, Amsterdam, The Netherlands. [11]University of Milan, Milan, Italy. [12]Department of Biomedical Engineering, Eindhoven University of Technology, Eindhoven, The Netherlands. ✉e-mail: irene.caffa@libero.it; w.zwart@nki.nl

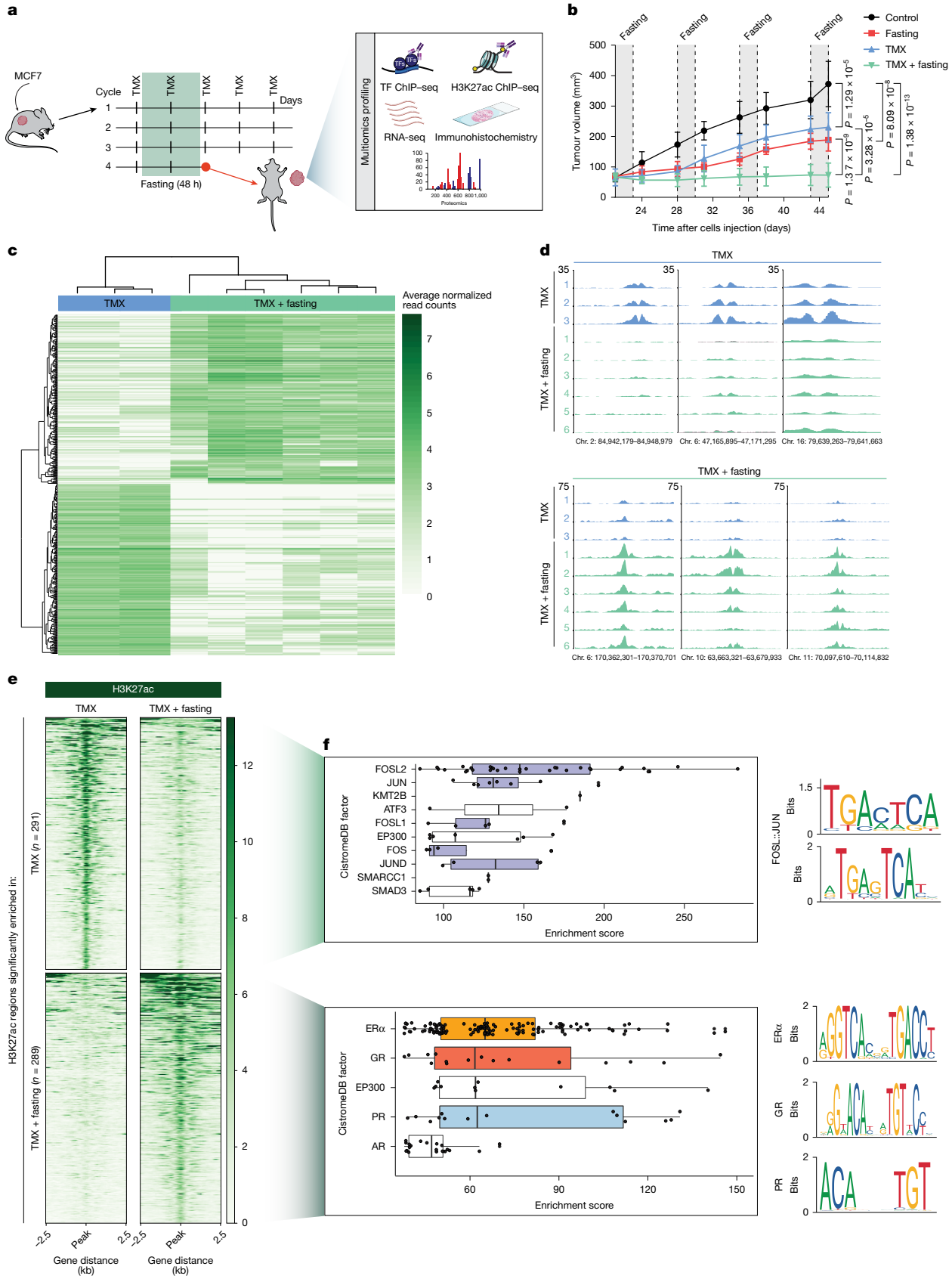

Fig. 1 | See next page for caption.

the active enhancer/promoter mark H3K27ac[9] and many transcription factors (Fig. 1a). A deep analysis of H3K27ac active enhancer/promoter profiles revealed profound epigenomic reprogramming in tumours collected from mice exposed to TMX plus fasting (Fig. 1c–e, Extended Data Fig. 1c–g and Extended Data Table 1) compared with those of tumours that were treated with TMX or fasting alone (Extended

Fig. 1 | Fasting induces H3K27ac changes in TMX-treated xenografts. **a**, Schematic representation of the treatment cycles of mice xenografted with MCF7 cells. After tumours reached a palpable size, mice were treated with the different treatment arms. After four weeks of treatment, tumours were collected and the represented multiomics profiling was performed. TF, transcription factor. Adapted from Servier Medical Art (https://smart.servier.com), CC BY 4.0. **b**, Xenograft tumour growth in six-to-eight-week-old female athymic nude mice randomized in control arm (ad libitum diet, $n = 6$) or fasting alone (48 h weekly, $n = 6$), TMX alone ($n = 6$) or TMX combined with fasting ($n = 6$) treatment arms. n represents number of tumours per treatment group. Data are mean ± s.e.m. P values by mixed-effect model with Tukey's multiple test correction (Supplementary Information) and two-tailed Student's t-test (P values from the last day are represented). **c**, Heat map depicting the differentially enriched H3K27ac regions between TMX alone ($n = 3$) or TMX plus fasting ($n = 6$). n represents number of tumours per treatment group. Colour scale represents the average normalized read counts. **d**, Representative snapshots of differentially enriched regions for H3K27ac between TMX (blue) and TMX plus fasting (green). The genomic coordinates are annotated. **e**, Heat map of differentially enriched H3K27ac signal in xenografts treated with TMX or TMX plus fasting. **f**, In silico GIGGLE analysis for factor enrichment at TMX-enriched H3K27ac sites (top left, $n = 3$) or TMX plus fasting-enriched H3K27ac sites (bottom left, $n = 6$). n represents number of tumours per treatment group. Right, average binding motifs of the depicted transcription factors, using HOMER software. In box plots, boxes indicate the first and third quartiles, the centre line indicates the median, and the whiskers indicate the first and third quartiles expanded by 1.5× the interquartile range (Supplementary Information).

Data Fig. 1c,d,f,g). To comprehensively identify transcription factors that potentially act through regulatory elements with altered epigenetic states after fasting, we intersected the genomic coordinates of fasting-affected H3K27ac sites in TMX-treated tumours with data from a publicly available ChIP–seq database[10] ($n = 13{,}976$) (Fig. 1f and Supplementary Information). H3K27ac sites with decreased signal upon fasting showed enriched occupancy for AP-1 transcription factor family members (including FOSL2, JUN, FOSL1, FOS and JUND)[11,12] (Fig. 1f, top), which are known to enhance breast cancer growth and proliferation[13]. In agreement with this finding, AP-1 inhibition effectively blocked proliferation of the HR$^+$ breast cancer cell lines MCF7 and T47D (Extended Data Fig. 1h), as previously reported[14]. The H3K27ac sites that were gained after fasting in TMX-treated tumours revealed an enrichment for ERα occupancy in silico (Fig. 1f, bottom), which was confirmed experimentally by ERα ChIP–seq in the same tumours (Extended Data Fig. 1i and Extended Data Table 1). Strong in silico enrichment at fasting-induced H3K27ac regions was also observed for other steroid hormone receptors (SHRs): GR, progesterone receptor (PR) and androgen receptor (AR). (Fig. 1f, bottom). All three SHRs serve as tumour suppressors in ERα$^+$ breast cancer[15–18], yet how their function is affected by dietary interventions remains unknown.

Fasting activates intratumoural GR and PR

Our in silico analyses suggested altered activity for many SHRs after fasting. To further explore the role of these SHRs in fasting-induced anti-tumour effects, we performed immunohistochemistry analysis to quantify the expression and subcellular localization of ERα, PR and GR in tumours collected from mice exposed to ad libitum diet, fasting, TMX or TMX plus fasting (Fig. 2a). We found that ERα and PR reside mostly in the nucleus, irrespective of their ligand state, as expected[17,19], and both their amount and subcellular localization were unaffected by fasting (Fig. 2a). By contrast, fasting—alone or in combination with TMX—strongly increased the nuclear localization of GR, an effect that is typically seen upon GR activation[20] (Fig. 2a).

SHRs exert their function by binding specific genomic regions to drive expression of their target genes. ChIP–seq analyses of GR and PR showed strong chromatin interactions upon fasting (Fig. 2b,c, Extended Data Fig. 2a,b and Extended Data Table 1). In line with our in silico predictions and motif enrichment analyses (Fig. 1f, bottom), H3K27ac regions that were enhanced with fasting were enriched for GR and PR occupancy, both after fasting alone and after fasting with TMX (Extended Data Fig. 2c). Whereas overall JUN chromatin binding was increased in tumours from fasted mice (Extended Data Fig. 2d and Extended Data Table 1), JUN binding was not observed in the newly engaged H3K27ac sites upon dietary intervention (Fig. 2d,e). When analysing sites that lost H3K27ac, we found that JUN occupancy remained unaltered. These data imply that fasting resulted in a loss of enhancer action at AP-1 sites, without affecting AP-1 chromatin binding at these sites. For newly gained enhancers, AP-1 was found not to occupy these regions, whereas both GR and PR did.

GR and PR are SHRs that depend on their cognate ligands for activation, namely cortisol (or corticosterone in mice) and progesterone, respectively. Therefore, we measured the levels of both hormones in mouse blood before and after the four-week treatment (which included four fasting cycles) (Fig. 2f,g) and in the serum of patients with breast cancer who were undergoing endocrine therapy in combination with a five-day FMD regimen as part of a clinical trial (ClinicalTrials.gov ID: NCT05748704) ($n = 15$) (Fig. 2h,i and Extended Data Table 2). In mice, fasting alone or fasting combined with TMX increased the concentrations of circulating corticosterone and progesterone (Fig. 2g and Extended Data Fig. 3a). Analogously, FMD also increased cortisol and progesterone levels in patients with breast cancer who were undergoing endocrine therapy (Fig. 2i), as well as in patients with breast cancer undergoing FMD without concomitant endocrine therapy in the DigesT study ($n = 35$; ClinicalTrials.gov ID: NCT03454282) (Fig. 2j). Fasting and FMDs were previously found to reduce blood IGF1, insulin and leptin concentrations (hereafter collectively referred to as fasting-reduced factors (FRFs)), in mice and humans with breast cancer[3,6,21,22]. The re-introduction of these FRFs reduced the beneficial effects of fasting on tumour growth[3] (Extended Data Fig. 3b) and prevented the increase of circulating corticosterone and progesterone levels in mice treated with TMX plus fasting (Extended Data Fig. 3a).

Collectively, these results indicate that fasting (in mice) and a FMD (in patients) increase the blood levels of cortisol and progesterone, promoting GR and PR activation in HR$^+$ breast cancer cells. Furthermore, fasting switches AP-1 occupied sites from an active epigenetic state to a repressed chromatin state, without affecting AP-1 binding.

Fasting activates GR-responsive genes

To understand the transcriptional consequences of an altered epigenome upon fasting, and whether and how such changes contribute to enhance endocrine therapy anti-tumour activity, we performed RNA-sequencing (RNA-seq) analyses. Consistent with the observed tumour regressions (Fig. 1b), RNA-seq analysis of MCF7 xenografts that were treated with TMX plus fasting revealed an inhibition of pathways related to cell proliferation (MYC[23] and E2F targets[24]) (Fig. 3a,b and Extended Data Fig. 3c,d). In agreement with our previous study[3], the nutrient sensor[25] mTOR showed decreased activity after fasting (Fig. 3b and Extended Data Fig. 3d). These data were confirmed by proteomic analysis (Extended Data Fig. 3e,f). Since fasting increased corticosteroid levels in mice and patients with HR$^+$ breast cancer (Fig. 2g,i,j) and increased chromatin binding of GR (Fig. 2b,c and Extended Data Fig. 2c), we utilized a pan-cancer applicable GR-activity gene signature[16] that confirmed elevated GR transcriptional activity in tumours collected from mice treated with TMX plus fasting (Fig. 3c). Unexpectedly, TMX treatment alone significantly reduced the expression of the GR-activity signature (Fig. 3c). GR activation was recently reported to exert anti-tumour effects in breast cancer by increasing the expression of the transcriptional suppressor ZBTB16 (also known as PLZF)[16]. Of note, *ZBTB16* was the second most

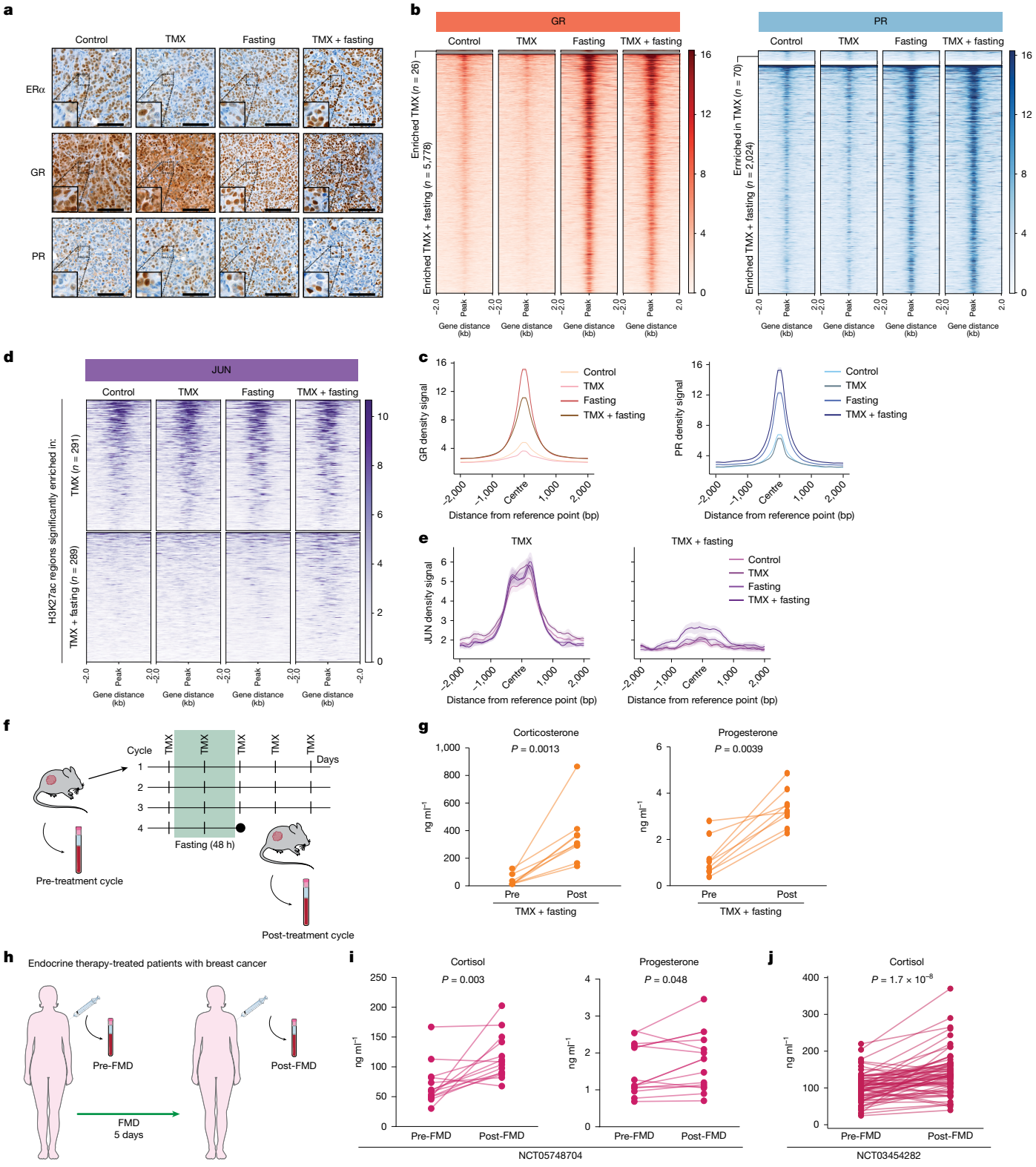

Fig. 2 | See next page for caption.

upregulated GR-signature gene in mice that received both TMX and weekly fasting cycles (Fig. 3d). Consistent with these findings, increased chromatin occupancy of both GR and PR was observed at the *ZBTB16* gene locus after fasting, which was accompanied by a marked increase in the active enhancer–promoter marker H3K27ac at the same site (Fig. 3e).

To confirm our xenograft-based observations in patients with breast cancer, we applied the same GR-activity signature to transcriptomic data derived from matched tumours specimens (pre- and post-FMD) from patients with HR$^+$ breast cancer undergoing a five-day FMD in the clinical trial NCT03454282. Consistent with the data obtained in mice, GR transcriptional activity was increased after FMD in these patient

Fig. 2 | Fasting enhances GR and PR chromatin binding and decreases enhancer activity at JUN sites. a, Representative immunohistochemistry staining for ERα, GR and PR in MCF7 xenografted tumours in the different treatment arms ($n = 4$). *n* represents number of mice per treatment group. Scale bars, 100 µm. **b**, Heat map depicting ChIP–seq signal for GR and PR in xenografts for all treatment arms. Regions altered in response to fasting in TMX-treated mice are shown. **c**, Average ChIP–seq signal for GR and PR for all conditions at sites that are enriched in the TMX plus fasting condition, with data centred on the peak, within a ±2-kb window. Data are mean ± s.e.m. **d**, ChIP–seq heat map signal for JUN in xenografts for all treatment conditions at H3K27ac regions that are differentially enriched in TMX and TMX plus fasting. **e**, Average JUN ChIP–seq signal for all conditions at H3K27ac regions that are enriched in TMX (left) and TMX plus fasting (right) conditions. Data are centred at the JUN peak, with a ± 2-kb window around the peak. Data are mean ± s.e.m. **f**, Schematic representation of blood collection schedule. Blood was collected from MCF7 xenografted mice before initiating the first cycle of fasting for all treatment conditions. Blood collection was repeated after the fourth cycle of fasting, when the mice were euthanized. Adapted from Servier Medical Art (https://smart.servier.com), CC BY 4.0. **g**, Corticosterone and progesterone levels in blood of mice before and after four cycles of TMX plus fasting ($n = 9$). *n* represents number of mice per treatment group. Data were analysed by two-tailed Wilcoxon signed rank test. **h**, Schematic representation of serum collection from patients with breast cancer who were being treated with endocrine therapy, before and after five days of FMD. Adapted from Servier Medical Art (https://smart.servier.com), CC BY 4.0. **i**, Cortisol and progesterone concentrations in serum of patients with ERα$^+$ breast cancer, as described in **h**. Data were analysed by two-tailed Student's paired *t*-test. **j**, Cortisol concentrations in serum of patients with ERα$^+$ breast cancer before and after five days of FMD. Data were analysed by two-tailed Student's paired *t*-test.

samples (Fig. 3f and Extended Data Fig. 4a,b). Moreover, we found that GR activity was negatively correlated with two Hallmark gene sets of tumour proliferation (Hallmark of E2F targets and G2M Checkpoint) (Fig. 3g). In line with the increased PR chromatin binding (Fig. 2b,c, Extended Data Fig. 2a,b and Extended Data Table 1) and the increased progesterone levels (Fig. 2g,i and Extended Data Fig. 3a), PR transcriptional activity was also increased in patients after FMD (Extended Data Fig. 4b,c and Extended Data Table 3).

Overall, these results indicate that fasting selectively activates transcriptional programmes that are under the control of GR and PR, both of which are known for their tumour suppressor function in HR$^+$ breast cancer[16,17].

GR activation mimics fasting effects

The beneficial effects of PR activation in HR$^+$ breast cancer have previously been reported[17] and are being explored in the phase 2 clinical trial PIONEER (ClinicalTrials.gov ID: NCT03306472). However, the role of GR activation in this type of cancer remains poorly understood. Here we focus on GR and its role in the enhancement of endocrine therapy activity through fasting. To determine whether the anti-proliferative effects of fasting are critically mediated by GR action, we knocked out GR in MCF7 cells (Extended Data Fig. 5a,b) and generated mouse xenografts from these GR-knockout (GR-KO) cells. As expected, GR-KO MCF7 cells did not respond to the GR agonist dexamethasone (Dexa) (Extended Data Fig. 5c–f). GR-KO and control MCF7 mouse xenografts were exposed to weekly 48 h fasting cycles, with or without TMX treatment (treatment schedule as in Fig. 1a). Whereas in control tumours, TMX and fasting synergistically blocked tumour growth (Fig. 4a,b and Extended Data Fig. 6a,b), confirming our previous observation[3] (Fig. 1b), this synergy was lost when GR was knocked out (Fig. 4a,b and Extended Data Fig. 6c,d).

Since GR appeared to have a central role in fasting-mediated enhancement of endocrine therapy for HR$^+$ breast cancer, we hypothesized that the beneficial effects of fasting could be mimicked by glucocorticoid administration. To test this hypothesis, we compared the anti-tumour activity of Dexa with fasting, alone or in combination with TMX, in MCF7 xenografts (Fig. 4c). Notably, combined Dexa and TMX phenocopied the anti-tumour activity of fasting plus TMX (Fig. 4d). Mice treated with Dexa did not undergo weight changes, whereas weight loss was observed in fasted mice (Extended Data Fig. 6e). The ability of Dexa to enhance endocrine therapy activity was further validated in a second HR$^+$ breast cancer xenograft model (T47D; Extended Data Fig. 6f,g) and in a HR$^+$ patient-derived xenograft (PDX) model (IDC186; Fig. 4e and Extended Data Fig. 6h,i). Consistent with the ability of combined fasting plus endocrine therapy to exert carry-over anti-tumour activity, we found that one month of treatment of MCF7 xenograft-bearing mice with Dexa plus TMX delayed tumour growth, after treatment withdrawal, by a factor of two, compared with fasting or TMX alone (Fig. 4f and Extended Data Fig. 7a).

We previously reported that fasting and FMDs lower insulin, IGF1 and leptin plasma concentrations in mice and humans with breast cancer[3,6,21,22]. Thus, we assessed whether the ability of Dexa to phenocopy the anti-tumour activity of fasting would reflect similar effects on these FRFs. Leptin and c-peptide were not affected, whereas serum IGF1 concentration decreased in response to Dexa (Extended Data Fig. 7b). Finally, in mice that were treated with TMX, Dexa attenuated TMX-induced uterus hyperplasia, a relatively common side effect of TMX, which we previously reported to be effectively prevented by fasting[3] (Extended Data Fig. 7c).

Dexamethasone is a potent immunomodulator, with significant adverse effects when chronically administered[26]. Therefore, we next determined whether the combined effect of Dexa and TMX might be less effective or even detrimental in an immunocompetent HR$^+$ breast cancer model, by affecting anti-tumour immunity. In allografts of the ERα$^+$ TSAE1 mouse breast cancer cell line[27,28] in BALB/c mice, combined treatment of Dexa with TMX significantly reduced tumour growth (Extended Data Fig. 7e,f) and increased the survival of these mice compared with TMX treatment alone (Fig. 4g).

To better understand whether and how treatment with Dexa would modulate the peripheral immune landscape, particularly with respect to the effects specific for TMX, we performed immune profiling of BALB/c mice bearing TSAE1 tumours from the different treatment groups (control, TMX, Dexa and TMX plus Dexa). We found no overt changes in leukocyte populations and in their proliferative capacities in response to the different treatments. However, combined Dexa plus TMX treatment led to a significant reduction in PD-L1 expression in neutrophils, non-classical monocytes and dendritic cells as compared with control treatment (Extended Data Fig. 7f).

Cumulatively, our findings indicate that the beneficial effects of fasting in enhancing endocrine therapy efficacy in breast cancer are mediated through GR activation, and that corticosteroid administration can be used to replace fasting to increase endocrine therapy activity.

Discussion

Dietary restriction represents a timely and promising research field in oncology. In particular, fasting or FMD regimens hold promise to achieve strong anti-tumour effects, with the ability to simultaneously activate multiple anti-tumour mechanisms[3]. Yet, concerns about the risk of malnutrition and impact on quality of life in relation to these diets remain. Thus, the search for fasting mimetics that could recreate its benefit in terms of anticancer effects is warranted. Our study defines GR agonists, such as Dexa, as a therapeutic intervention that phenocopies the beneficial effects of fasting, enhancing endocrine therapy efficacy. GR agonists have been used in the clinic for decades, including as anticancer agents (for example, for haematological malignancies such as lymphomas or multiple myeloma), anti-inflammatory and anti-allergic drugs, and antiemetics. However, their prescription as

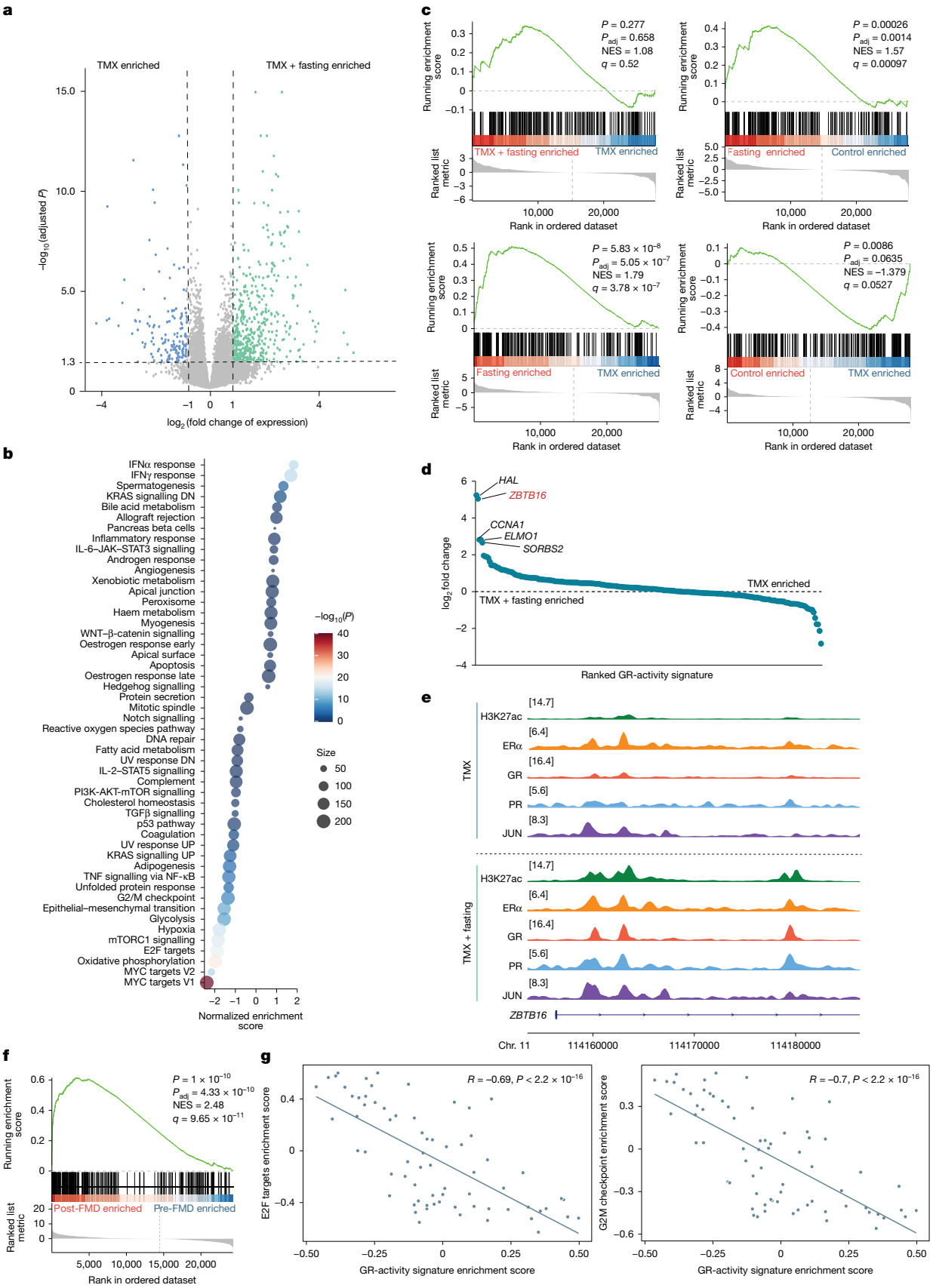

Fig. 3 | See next page for caption.

Fig. 3 | Fasting enhances GR transcriptional activity and increases expression of the transcriptional suppressor *ZBTB16*. **a**, Volcano plot depicting genes that are differentially expressed between TMX and TMX plus fasting treated MCF7 xenografts. Differential gene expression was determined by two-sided Wald test. **b**, Gene set enrichment analysis for Hallmark pathways. Shown are the pathways that are differentially enriched upon treatment with TMX or TMX plus fasting. Normalized enrichment score (NES) was calculated by weighted Kolmogorov–Smirnov test and *P* value was determined by permutation-based testing with multiple Benjamini–Hochberg hypothesis correction. DN, downregulation; UP, upregulation. **c**, Enrichment plot of a pan-cancer GR-activity signature for all depicted conditions. NES was calculated by weighted Kolmogorov–Smirnov test and *P* value determined by permutation-based testing with multiple Benjamini–Hochberg hypothesis correction. **d**, Differential expression analyses for GR-activity signature genes, based on $\log_2$-transformed fold change ranking, comparing TMX and TMX plus fasting conditions. **e**, Snapshots of H3K27ac, ERα, GR, PR and JUN ChIP–seq signal at the *ZBTB16* gene locus in TMX-treated and TMX plus fasting-treated xenografts. **f**, Enrichment plot for GR-activity signature in matched tumour samples of patients with breast cancer, before and after five days of FMD. NES was calculated by weighted Kolmogorov–Smirnov test and *P* value was determined by permutation-based testing with multiple Benjamini–Hochberg hypothesis correction. **g**, Correlation plot between of G2M and E2F Hallmarks, and the GR-activity signature in matched tumour samples from patients with breast cancer, before and after five days of FMD. Two-sided Spearman's linear correlation between gene set variation analysis (GSVA) enrichment scores of the indicated gene sets was calculated, and *R* and *P* values are shown.

drugs that can modify the activity of endocrine therapy for HR$^+$ breast cancer in currently not foreseen.

Fasting has direct metabolic consequences, such as lower serum glucose, decreased insulin levels and, consequently, decreased AKT–mTOR signalling, which have been attributed anti-tumour effects[3], including in breast cancer. Our data show that the ability of fasting to enhance the anti-tumour effects of endocrine therapy for breast cancer is largely mediated through GR signalling. SHRs show substantial genomic crosstalk in breast cancer cells. In particular, GR, AR and PR all share genomic regions with ERα throughout the genome[29] and serve as tumour suppressors in HR$^+$ breast cancer[16–18]. Although the crosstalk between SHRs has been studied extensively at the biological level, suggesting novel therapeutic opportunities in breast cancer treatment[17], the physiological causes of this interplay remain unknown. We show here that fasting increases levels of cortisol (or corticosterone) and progesterone, selectively activating GR and PR genetic programmes, to increase the effect of endocrine therapy in breast cancer (Fig. 4h).

PR agonist treatment is being evaluated in combination with letrozole in a phase 2 randomized clinical trial in patients with ERα$^+$ breast cancer (ClinicalTrials.gov ID: NCT03306472). However, the MIPRA clinical trial showed that PR inhibition by mifepristone also reduced tumour cell proliferation in patients with HR$^+$ breast cancer (ClinicalTrials.gov ID: NCT02651844)[30]. These contradictory results can be partially explained by the use of mifepristone, which is a potent PR inhibitor but, when used at high doses or depending on the time of the day when the drug is taken (night versus morning), also acts as a GR agonist[31–33]. GR activation promotes a luminal HR$^+$ breast cancer phenotype associated with improved prognosis and reduced cell proliferation[16]. Here we show that GR activation enhances the effects of the endocrine therapy, and exogenously administered GR agonists phenocopy the favourable effects of fasting.

Chronic treatment with corticosteroids may exert undesirable effects on the immune system, bones, muscles and endocrine system[26]. Our in vivo studies using an immunocompetent mice model revealed that Dexa significantly delayed tumour growth and extended survival of mice bearing an HR$^+$ tumour compared with TMX alone (Fig. 4g). Moreover, immune profiling of these mice indicated a balanced immune state, with no signs of pronounced activation or suppression. We observed a significant reduction in PD-L1 expression in some immune cell populations when Dexa was combined with TMX (Extended Data Fig. 7f). Since low PD-L1 expression is considered to be a marker of immune cell activation and increased anticancer activity of the immune system[34], it is possible that the anti-tumour effects that we observed with TMX plus Dexa in this immunocompetent mouse breast cancer model also reflected favourable systemic effects of Dexa on anti-tumour immunity, although this mechanism needs to be confirmed through further studies.

GR stimulation is most effective at decreasing breast cancer cell proliferation in the luminal A patient population[16], which is consistent with our data. Several clinical trials from the late 1980s and early 1990s evaluated the therapeutic contribution of glucocorticoids to endocrine therapy in patients with breast cancer, finding that the glucocorticoids only modestly improved response rates[35–37]. However, these clinical trials enrolled patients with unknown receptor status. Since GR agonism drives tumour migration and proliferation in triple-negative breast cancer[38], the limited benefit of glucocorticoid administration in the earlier studies may be explained by the enrollment of a significant fraction of patients with triple-negative breast cancer[35–37].

Our study positions glucocorticoid administration as a novel therapeutic strategy that mimics the effects of fasting in HR$^+$ breast cancer cancer treatment, substituting the need for dietary restriction with a clinically approved and safe therapeutic agent.

Online content

Any methods, additional references, Nature Portfolio reporting summaries, source data, extended data, supplementary information, acknowledgements, peer review information; details of author contributions and competing interests; and statements of data and code availability are available at https://doi.org/10.1038/s41586-025-09869-0.

1. Burstein, H. J. Systemic therapy for estrogen receptor-positive, HER2-negative breast cancer. *N. Engl. J. Med.* **383**, 2557–2570 (2020).
2. Pan, H. et al. 20-year risks of breast-cancer recurrence after stopping endocrine therapy at 5 Years. *N. Engl. J. Med.* **377**, 1836–1846 (2017).
3. Caffa, I. et al. Fasting-mimicking diet and hormone therapy induce breast cancer regression. *Nature* **583**, 620–624 (2020).
4. Koppold, D. A. et al. International consensus on fasting terminology. *Cell Metab.* **36**, 1779–1794.e1774 (2024).
5. Valdemarin, F. et al. Safety and feasibility of fasting-mimicking diet and effects on nutritional status and circulating metabolic and inflammatory factors in cancer patients undergoing active treatment. *Cancers* **13**, 4013 (2021).
6. Vernieri, C. et al. Fasting-mimicking diet is safe and reshapes metabolism and antitumor immunity in patients with cancer. *Cancer Discov.* **12**, 90–107 (2022).
7. Vernieri, C., Ligorio, F., Tripathy, D. & Longo, V. D. Cyclic fasting-mimicking diet in cancer treatment: Preclinical and clinical evidence. *Cell Metab,* **36**, 1644–1667 (2024).
8. Burstein, H. J. et al. Adjuvant endocrine therapy for women with hormone receptor–positive breast cancer: ASCO clinical practice guideline focused update. *J. Clin. Oncol.* **37**, 423–438 (2018).
9. Creyghton, M. P. et al. Histone H3K27ac separates active from poised enhancers and predicts developmental state. *Proc. Natl Acad. Sci. USA* **107**, 21931–21936 (2010).
10. Zheng, R. et al. Cistrome Data Browser: expanded datasets and new tools for gene regulatory analysis. *Nucleic Acids Res.* **47**, D729–d735 (2019).
11. Angel, P. & Karin, M. The role of Jun, Fos and the AP-1 complex in cell-proliferation and transformation. *Biochim. Biophys. Acta* **1072**, 129–157 (1991).
12. Shaulian, E. & Karin, M. AP-1 in cell proliferation and survival. *Oncogene* **20**, 2390–2400 (2001).
13. Shen, Q. et al. The AP-1 transcription factor regulates breast cancer cell growth via cyclins and E2F factors. *Oncogene* **27**, 366–377 (2008).
14. Fanjul, A. et al. A new class of retinoids with selective inhibition of AP-1 inhibits proliferation. *Nature* **372**, 107–111 (1994).
15. Tonsing-Carter, E. et al. Glucocorticoid receptor modulation decreases ER-positive breast cancer cell proliferation and suppresses wild-type and mutant ER chromatin association. *Breast Cancer Res.* **21**, 82 (2019).
16. Prekovic, S. et al. Luminal breast cancer identity is determined by loss of glucocorticoid receptor activity. *EMBO Mol. Med.* **15**, e17737 (2023).
17. Mohammed, H. et al. Progesterone receptor modulates ERα action in breast cancer. *Nature* **523**, 313–317 (2015).
18. Hickey, T. E. et al. The androgen receptor is a tumor suppressor in estrogen receptor-positive breast cancer. *Nat. Med.* **27**, 310–320 (2021).
19. Kocanova, S., Mazaheri, M., Caze-Subra, S. & Bystricky, K. Ligands specify estrogen receptor alpha nuclear localization and degradation. *BMC Cell Biol.* **11**, 98 (2010).
20. Stortz, M. et al. Mapping the dynamics of the glucocorticoid receptor within the nuclear landscape. *Sci. Rep.* **7**, 6219 (2017).

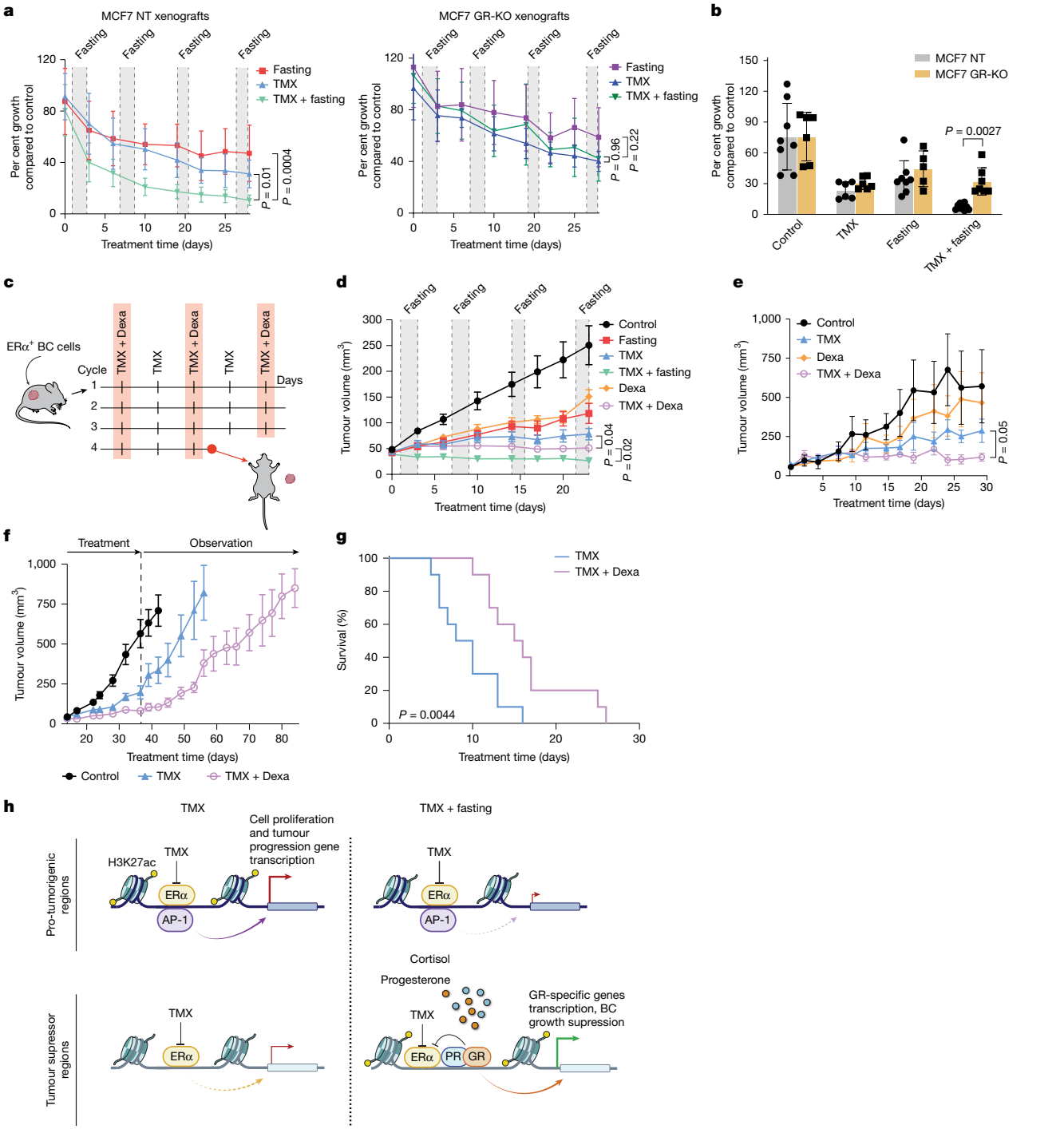

Fig. 4 | GR activity drives beneficial effects of fasting in endocrine response. **a**, Non-targeted control (NT) or GR-KO MCF7 xenograft tumour growth in six-to-eight-week-old female athymic nude mice treated with fasting (NT, $n = 8$; GR-KO, $n = 6$), TMX (NT, $n = 9$; GR-KO, $n = 7$) and TMX plus fasting (NT, $n = 11$; GR-KO, $n = 9$). Tumour growth was normalized to the respective control tumours **b**, Per cent MCF7 NT or GR-KO tumour volume compared with the respective control (control: NT, $n = 8$; GR-KO, $n = 6$; fasting: NT, $n = 8$; GR-KO, $n = 5$; TMX: NT, $n = 6$; GR-KO, $n = 6$; TMX plus fasting: NT, $n = 10$; GR-KO, $n = 7$). Data are mean ± s.d. Comparison by two-sided Student's *t*-test on the last day. **c**, Schematic representation of the four treatment cycles. Mice were randomized into control arm, Dexa, TMX or TMX plus Dexa treatment arms. BC, breast cancer. Adapted from Servier Medical Art (https://smart.servier.com), CC BY 4.0. **d**, MCF7 xenograft outgrowth in six-to-eight-week-old female athymic nude mice in the different treatment arms (control, $n = 8$; TMX, $n = 9$; Dexa, $n = 6$; fasting, $n = 8$; TMX plus fasting, $n = 11$; TMX plus Dexa, $n = 7$). **e**, HR$^+$ breast cancer PDX outgrowth in six-to-eight-week-old female NSG mice in the different treatment arms (control, $n = 4$; TMX, $n = 4$; Dexa, $n = 4$; TMX plus Dexa, $n = 5$). **f**, MCF7 xenograft outgrowth in six-to-eight-week-old female athymic nude mice in the different treatment arms (control, $n = 7$; TMX, $n = 7$; Dexa, $n = 5$; TMX plus Dexa, $n = 6$). After four weeks, all treatments were stopped and tumours were allowed to re-grow. Data are mean ± s.e.m. **g**. Survival curves of immunocompetent mice engrafted with TSAE1 cells and treated with either TMX alone ($n = 10$) or combined with Dexa ($n = 10$). Log-rank test is depicted. **h**. Proposed model for fasting-enhanced TMX response in breast cancer cells. **a**,**b**,**d**–**g**, *n*, number of tumours per treatment group. **a**,**d**,**e**, Data are mean ± s.e.m. *P* values by mixed-effect model with Tukey's multiple test correction (Supplementary Information) and two-tailed Student's *t*-test (*P* values of last day are represented).

21. Salvadori, G. et al. Fasting-mimicking diet blocks triple-negative breast cancer and cancer stem cell escape. *Cell Metab.* **33**, 2247–2259.e2246 (2021).
22. Ligorio, F. et al. Early downmodulation of tumor glycolysis predicts response to fasting-mimicking diet in triple-negative breast cancer patients. *Cell Metab.* **37**, 330–344.e337 (2025).
23. Schulze, A., Oshi, M., Endo, I. & Takabe, K. MYC targets scores are associated with cancer aggressiveness and poor survival in ER-positive primary and metastatic breast cancer. *Int. J. Mol. Sci.* **21**, 8127 (2020).
24. Oshi, M. et al. The E2F pathway score as a predictive biomarker of response to neoadjuvant therapy in ER+/HER2− breast cancer. *Cells* **9**, 1643 (2020).
25. Fernandes, S. A. & Demetriades, C. The multifaceted role of nutrient sensing and mTORC1 signaling in physiology and aging. *Front. Aging* **2**, 707372 (2021).
26. Buchman, A. L. Side effects of corticosteroid therapy. *J. Clin. Gastroenterol.* **33**, 289–294 (2001).
27. Lollini, P. L. et al. High-metastatic clones selected in vitro from a recent spontaneous BALB/c mammary adenocarcinoma cell line. *Clin. Exp. Metastasis* **2**, 251–259 (1984).
28. Turrell, F. K. et al. Age-associated microenvironmental changes highlight the role of PDGF-C in ER+ breast cancer metastatic relapse. *Nat. Cancer* **4**, 468–484 (2023).
29. Mayayo-Peralta, I., Prekovic, S. & Zwart, W. Estrogen receptor on the move: cistromic plasticity and its implications in breast cancer. *Mol. Aspects Med.* **78**, 100939 (2021).
30. Elía, A. et al. Beneficial effects of mifepristone treatment in patients with breast cancer selected by the progesterone receptor isoform ratio: results from the MIPRA trial. *Clin. Cancer Res.* **29**, 866–877 (2023).
31. Meijer, O. C. et al. Steroid receptor coactivator-1 splice variants differentially affect corticosteroid receptor signaling. *Endocrinology* **146**, 1438–1448 (2005).
32. Havel, P. J. et al. Predominately glucocorticoid agonist actions of RU-486 in young specific-pathogen-free Zucker rats. *Am. J. Physiol.* **271**, R710–R717 (1996).
33. Besedovsky, L., Born, J. & Lange, T. Endogenous glucocorticoid receptor signaling drives rhythmic changes in human T-cell subset numbers and the expression of the chemokine receptor CXCR4. *FASEB J.* **28**, 67–75 (2014).
34. Butte, M. J., Keir, M. E., Phamduy, T. B., Sharpe, A. H. & Freeman, G. J. Programmed death-1 ligand 1 interacts specifically with the B7-1 costimulatory molecule to inhibit T cell responses. *Immunity* **27**, 111–122 (2007).
35. Keith, B. D. Systematic review of the clinical effect of glucocorticoids on nonhematologic malignancy. *BMC Cancer* **8**, 84 (2008).
36. Rubens, R. D. et al. Prednisolone improves the response to primary endocrine treatment for advanced breast cancer. *Br. J. Cancer* **58**, 626–630 (1988).
37. Stewart, J. F. et al. Contribution of prednisolone to the primary endocrine treatment of advanced breast cancer. *Eur. J. Cancer Clin. Oncol.* **18**, 1307–1314 (1982).
38. Obradović, M. M. S. et al. Glucocorticoids promote breast cancer metastasis. *Nature* **567**, 540–544 (2019).

Methods

Animal experiments

All mouse experiments were performed in accordance with institutional guidelines for animal care and use established in the Principles of Laboratory Animal Care (directive 86/609/EEC). Animal work was only initiated upon approval by the Italian Istituto Superiore di Sanità (ISS) with authorization no. 40/2022, protocol 22418.167 or by the Animal Ethics Committee of the Netherlands Cancer Institute. Six-to-eight-week-old female athymic nude mice (purchased from Envigo) were used in the experiments at the Animal Facility of the IRCCS Ospedale Policlinico San Martino (Genoa). These mice were housed in Sealsafe Plus GM500 individually ventilated cages (IVCs) held on DGM Racks at 22 ± 2 °C and approximately 50–60% relative humidity under a 12 h:12 h light:dark lighting cycle and with food (standard diet, 4RF18, Mucedola) and water ad libitum. Mice were acclimatized for one week before experiments were initiated. To allow MCF7 xenograft growth, a 17β-oestradiol-releasing pellet (Innovative Research of America) was inserted in the intra-scapular subcutaneous region under anaesthesia conditions, the day before cell injection. Xenografts were established by subcutaneous injection of 5×10^6 MCF7 cells to both flanks of the mouse (experiments in Figs. 1a,b, 2 and 4a,b), or orthotopic injection of 3×10^6 MCF7 cells into the fourth abdominal fat pad (experiments in Fig. 4d and Extended Data Fig. 3a,b). Treatment was initiated when the tumours appeared as established palpable masses (~2 weeks after cell injection). In each experiment, mice were randomly assigned to receive one of the following treatments or their combinations, as indicated: control (ad libitum diet); TMX (45 mg kg^{-1} per day in peanut oil, oral gavage[3,39]), fasting (water only, for 48 h every week[3,40]), Dexa (4 mg kg^{-1} every other day in physiological solution, intraperitoneal[41]), IGF1 (200 µg kg^{-1} body weight, intraperitoneal twice a day on the days of fasting); insulin (20 mU kg^{-1} body weight, intraperitoneal once a day on the days of fasting); leptin (1 mg kg^{-1} body weight, intraperitoneal once a day on the day of fasting). During the 48 h of fasting, mice were individually housed in a clean, new cage to reduce coprophagy and the intake of the residual chow. Body weight was measured immediately before, during and after fasting. Fasting cycles were repeated every seven days to allow for complete recovery of body weight before a new cycle. The size of the tumours was measured twice a week and tumour volume was calculated using the formula: tumour volume (in mm^3) = $(w^2 \times W) \times \pi/6$, where w and W are lengths of the minor side and major side (in mm), respectively. The maximum tumour volume that was permitted by our Institutional Animal Care and Use Committee (IACUC) was 1,500 mm^3, and in none of the experiments were these limits exceeded. Tumour masses were isolated at the end of the last fasting cycle, weighed, divided into two parts, snap frozen in liquid nitrogen and stored at −80 °C. Ten slices of 50 µm per tumour sample were subsequently utilized for ChIP–seq, proteomics and RNA-seq analyses. Sample size estimation was performed using PS (power and sample size calculation) software (Vanderbilt University). By this approach, we estimated that the number of mice that were assigned to each treatment group would reach a power of 0.85. The type I error probability associated with our tests of the null hypothesis was 0.05. Mice were assigned to the different experimental groups in a random fashion. Operators were unblinded, as blinding during animal experiments was not possible because mice were subject to a specific diet supply and daily treatment.

To establish mammary intraductal cell line-derived xenograft (MIND-CDX) models, T47D cells were intraductally injected as previously described[39,42]. Specifically, 1×10^6 T47D cells were dissociated to single cells with 0.05% trypsin and injected intraductally into the abdominal/inguinal mammary glands (both sides) of 8-week-old female NSG mice (Jackson Laboratory) with a 34G needle. To ensure stable outgrowth, T47D MIND-CDX mice were supplemented with 17β-oestradiol (Sigma, E2758) via the drinking water at a concentration of 4 µg ml^{-1} starting 7 days prior to tumour inoculation via intraductal injection. E2 supplementation was maintained throughout the experiment. To establish TSAE1 allograft models, BALB/c mice (Jackson Laboratory) were intraductally injected with of 1×10^4 single cells in PBS as described above (one gland). The IDC186 MIND-PDX model was established from a pre-menopausal Caucasian breast cancer patient, confirmed positive for ERα (95%) and PR (95%) but negative for HER2 (Extended Data Fig. 6h). To generate the PDX model, 5×10^4 single cells in PBS were intraductally injected into one of the abdominal mammary glands of 8-week-old female NSG mice (Jackson Laboratory) and supplemented with 17β-oestradiol (Sigma, E2758) as described above.

The xenograft model cohorts were monitored three times per week and tumours were palpated and measured via calliper in two dimensions. Mice were enrolled into treatment groups when the largest tumour per animal measured 50 mm^3 for T47D and IDC186 xenografts and 25 mm^3 for TSAE1 allografts, respectively. Mice were randomly allocated into treatment groups and received the following treatments: (1) vehicle treatment (corn oil, daily, oral gavage); (2) TMX (45 mg kg^{-1} in corn oil, daily, oral gavage); (3) Dexa (4 mg kg^{-1}, 3 times per week, intraperitoneal injection); or (4) TMX plus Dexa. Mice were treated for 28 consecutive days for the TSAE1 and IDC186, 56 days for T47D (with a 1-week treatment break between days 28 and 35), or until the cumulative mammary tumour burden reached a volume of 1,500 mm^3 and thus the maximally permitted disease end point. At euthanasia, mammary glands and full female reproductive tracts were collected in formalin, stained against haematoxylin and eosin (H&E) according to routine procedures, and uteri were analysed for histopathological abnormalities. Tumour measurements and post-mortem analysis were performed in blinded fashion. H&E slides were reviewed by a trained pathologist (J.-Y.S.) in a blinded manner. Slides were digitally processed using a PANNORAMIC 1000 whole slide scanner (3DHISTECH) and captured with the Slidescore software (www.slidescore.com).

Clinical studies of FMD in patients undergoing endocrine therapy for HR^+ breast cancer

The NCT05748704 trial was conducted at the IRCCS Ospedale Policlinico San Martino (Genoa), between December 2022 and February 2024 and was approved by the Comitato Etico Regione Liguria. This trial consists of a single-arm phase I/II clinical study of a FMD with solid tumours who are candidates to receive active medical or radiotherapy treatment (or with medical treatment or radiotherapy already ongoing). The nutritional intervention consists of a low-calorie diet lasting 5 days and aimed at providing between 800 and 1,000 kcal day^{-1} (tentatively 10% carbohydrates, 15% proteins and 75% lipids). Throughout the clinical study, patients have received dietary counselling for the intervals between FMD cycles, aiming at providing an appropriate intake of proteins, essential fatty acids, vitamins and minerals[43] and have also been invited to perform light/ or moderate daily muscle training to enhance muscle anabolism[44]. Study primary outcomes were the effects of the FMD regimen on the circulating levels of factors with pro- or anti-oncogenic activity (including insulin, IGF1, IGFBP1, IGFBP3, leptin, adiponectin, IL-6, TNF and IL-1β), as well as the effect of FMD cycles on leukocyte subpopulations with a role in tumour growth control, such as regulatory T cells, myeloid-derived suppressor cells (MDSCs) as well as natural killer (NK) cells, and its stem cell pool (for example, haematopoietic stem cells, endothelial stem cells, mesenchymal stem cells). Additional information on this trial is available at https://clinicaltrials.gov/ct2/show/NCT05748704. Patient serum for subsequent ELISA assays of circulating growth factors and adipokines has been routinely collected before and after the first, sixth and twelfth FMD cycle. Informed consent was obtained from all patients participating in the clinical trial.

The DigesT study (ClinicalTrials.gov ID: NCT03454282) trial was conducted between July 2018 and December 2020 and in accordance with the Declaration of Helsinki and the principles of Good Clinical

Practice. The study protocol was approved by the Institutional Review Board (IRB) and the Ethics Committee of Fondazione IRCCS Istituto Nazionale dei Tumori Milan (INT 157/17). All patients provided written informed consent before any study procedures, as well as for the use of clinical and biological data for research purpose. The FMD nutritional intervention consisted in a 5-day, plant-based, calorie-restricted (up to 600 kcal on day 1; up to 300 kcal on days 2, 3, 4 and 5), low-carbohydrate, low-protein, nutritional regimen, as previously published[6]. Enrolled patients initiated the FMD 12–15 days before surgery, and underwent blood sampling after at least 8 h complete fasting on the morning (08:30 to 10:00) of FMD initiation (pre-FMD), and on the morning of FMD completion (post-FMD). Tumour samples for RNA-seq analyses were obtained diagnostic core biopsies performed at baseline (Pre-) and from matched surgical specimens (Post-). The primary outcomes of the study were to measure the absolute and relative changes in population of peripheral blood mononuclear cells before and after the FMD. Additional information on this trial is available at https://clinicaltrials.gov/ct2/show/NCT03454282.

ChIP–seq

Snap-frozen xenografted tumours were double fixed using 2 mM of disuccinimidyl glutarate diluted in solution A (50 mM Hepes, 100 mM NaCl, 1 mM EDTA, 0.5 mM EGTA) for 25 min followed by 1% formaldehyde for 20 min, at room temperature. Cells were then lysed and sonicated accordingly to the protocol previously described[45], with the difference of have performed 15 cycles of 30 s on, 30 s off in the sonication step (BioRuptor Pico, Diagenode). Obtained nuclear lysates were incubated overnight with 50 µl of protein A coated Dynabeads magnetic beads (10008D, Invitrogen) conjugated with 5 µg of ERα (06-935, Millipore), H3K27ac (39133, Active Motif), GR (12041S, Cell Signaling), PR (8757S, Cell Signaling) or JUN (9165S, Cell Signaling) antibodies. The resulting immunoprecipitated DNA was submitted for library preparation using the KAPA library kit (KK8234, Roche) and subsequently paired-end sequenced on the Illumina NovaSeq 6000 system with read length of 51 bp. ChIP–seq analyses were performed using an in house pipeline publicly available at https://github.com/sebastian-gregoricchio/ChIP_Zwart (v.0.1.2) with default parameters. In brief, all samples were aligned to reference genome Hg38/GRCh38 using Burrows-Wheeler Aligner[46] (BWA v.0.5.10). Reads were filtered based on mapping quality (MAPQ ≥ 20), and duplicate reads were marked with Picard MarkDuplicates (v.2.19.0). MACS2 (v.2.1.2) was used to perform peak calling over input ChIP–seq samples; only peaks with a q-value < 0.01 were retained. DeepTools[47] (v.2.5.3) was used to calculate the fraction of reads in peaks (FRiP) and normalized ChIP–seq signal. For visualization purposes, Reads Per Genomic Content (RPGC) normalization (1× coverage) signal was averaged among the replicates per each condition using deeptools bigwigCompare. Genome browser snapshots were generated using the R v.4.0.3 environment and Rseb[48] (v.0.3.1) (https://github.com/sebastian-gregoricchio/Rseb). Tornado plots were generated using deepTools (v.2.5.3). Differential peak analyses were performed using diffBind[49] (v.3.0.15). Peaks were defined as differential when the $|\log_2(\text{fold change})| > 1.5$ and adjusted P value <0.05. Genomic location annotation of the peaks was performed using ChIPSeeker[50] (v.1.26.2) defining the promoter region as −2 kb:transcription start site:+1 kb. Transcription factor binding enrichment from public available datasets—GIGGLE analyses[51]—were performed using the tool available at the of CistromeDB website (http://cistrome.org/db/).

Cell lines

The MCF7, T47D and HEK293T cell lines were purchased from the American Type Culture Collection (ATCC). TSAE1 cells were a gift from C. Isacke laboratory[28]. All cell lines were kept in DMEM, high glucose, pyruvate (Gibco) and supplemented with 10% fetal bovine serum (FBS, Capricorn Scientific) and 1% penicillin-streptomycin (5,000 U ml^{-1}, Life Technologies). For ligand treatment, 4-hydroxytamoxifen (HY16950; MedChemExpress) and SR11302 (HY-15870; MedChemExpress) were reconstituted in DMSO, and used in the described concentrations and time points. All cell lines were cultured at 5% CO_2 at 37 °C, were subjected to regular Mycoplasma testing, and underwent authentication by short tandem repeat profiling (Eurofins Genomics).

CRISPR–Cas9-mediated knockout cell line generation

GR-targeting single-guide RNA (*NR3C1*; ATGACTACGCTCAACATGTT) and non-targeting (NT) control guide RNA (GTATTACTGATATTG GTGGG) were separately cloned into the lentiCRISPR v.2 vector[52]. Using H3K293T cells, the CRISPR vectors were co-transfected with third-generation viral vectors using polyethyleneimine (PEI, Polysciences). After lentivirus production, the medium was collected and added to the MCF7 cells. Two days after infection, cells were selected for 2 weeks with 2 µg ml^{-1} puromycin (Sigma Aldrich), and knockout efficiency was confirmed by western blot and immunofluorescence.

Immunoblotting

Total protein lysates were obtained using Laemmli buffer complemented with 1× complete protease inhibitor cocktail (Roche) and 1× phenylmethylsulfonyl fluoride (PMSF). Forty micrograms of protein per sample was resolved in a NuPAGE 4–12% Bis-Tris gel (NP0335BOX, Invitrogen) in 1× NuPAGE MOPS SDS Running Buffer (NP00012, Invitrogen) and sequentially transferred to a 0.45-µm nitrocellulose membrane (Santa Cruz Biotechnology). Protein detection was performed using antibodies raised to detect GR (1:1,000, 12041S, Cell Signaling) and β-actin (1:10,000, MAB1501R, Merck Millipore). Odyssey CLx Imaging system (Li-Cor Biosciences) and ImageStudio Lite v.5.2.5 (LI-COR Biosciences) software were used to scan and visualize the proteins.

Immunofluorescence

Cells were fixed with 2% paraformaldehyde (103999, Merck) for 10 min, washed twice with PBS and subsequently permeabilized with 0.5% Triton/PBS (Triton X-100, Sigma Aldrich). Following two PBS washing steps, cells were blocked for 1 h in 1% bovine serum albumin (BSA, A8022, Sigma/Merck)/PBS solution before incubation with antibody against GR (1:100, 12041S, Cell Signaling). After two additional PBS washes, cells were incubated with Alexa Fluor 488 goat anti-rabbit IgG (1:1,000, A-11008, ThermoFisher Scientific) and DAPI (ProLong Gold Antifade Mountant, P36930, ThermoFisher Scientific) and signal detected using laser confocal microscopy (SP5, Leica).

Immunohistochemistry

Immunohistochemistry of the formalin-fixed, paraffin-embedded (FFPE) tumour samples was performed on a BenchMark Ultra (Ki-67) or a Discovery Ultra (ERα, PR, GR) automated stainer (Ventana Medical Systems). In brief, paraffin sections were cut at 3 µm, heated at 75 °C for 28 min and deparaffinised in the instrument with EZ prep solution (Ventana Medical Systems). Heat-induced antigen retrieval was carried out using Cell Conditioning 1 (CC1, Ventana Medical Systems) for 32 min (Ki-67, ERα, PR) or 64 min (GR) at 95 °C. Ki-67 was detected using the clone 30-9 (Ready-to-Use, 32 min at 37 °C, Roche Diagnostics/Ventana), GR using the clone D6H2L (1/600 dilution, 1 h at 37 °C, 12041, Cell Signalling), ERα using the clone SP1 (Ready-to-Use, 32 min at room temperature, Roche Diagnostics/Ventana) and PR using the clone 1E2 (Ready-to-Use, 32 min at room temperature, Roche Diagnostics/Ventana). In order to reduce background signal for the PR staining, after primary antibody incubation slides were incubated with normal antibody diluent (Roche Diagnostics) for 24 min. Bound Ki-67 antibody was detected using the OptiView DAB Detection Kit (Ventana Medical Systems). GR and ERα bound antibody was visualized using Anti-Rabbit HQ (Ventana Medical systems) for 12 min at 37 °C followed by Anti-HQ HRP (Ventana Medical systems) for 12 min at 37 °C and the ChromoMap

DAB detection kit (Ventana Medical Systems). PR bound antibody was detected using OmniMap anti-Rabbit HRP (Ventana Medical systems) for 12 min at room temperature. followed by ChromoMap DAB detection kit (Ventana Medical Systems). Slides were counterstained with Hematoxylin and Bluing Reagent (Ventana Medical Systems). A PANNORAMIC 1000 scanner from 3DHISTECH was used to scan the slides at a 40× magnification and uploaded to the Slidescore software (www.slidescore.com). Digitized slides were further processed using QuPath (v.0.6.0)[53]. The analysis protocol begins with tissue detection using a pixel classifier, which differentiates foreground from background (white) pixels. Next, manual annotation is performed with the brush tool to delineate and exclude stroma areas from the region of interest. To identify Ki-67-positive and negative cells, the native cell detection tool is used with the optical density sum option for image analysis. Default parameters are applied, with adjustments made only to the pixel size (0.25 µm), based on the slide resolution, and the target cell size (8 µm) for accurate cell identification. Finally, the scoring is calculated as the proportion of positive cells relative to the total number of detected cells, providing a quantitative assessment of Ki-67 expression. All quantifications were compared and approved by a trained pathologist (J.S.).

RNA-seq analyses

MCF7 xenograft tumour RNA was isolated by homogenizing the tissue sample in 1 ml of RLT buffer (79216, Qiagen) and 1% β-mercaptoethanol using the Qiagen TissueLyserII (85300, Qiagen) for 6 min with frequency setting 30 (1 s^{-1}) in combination with 5-mm stainless steel beads (69989, Qiagen). The total RNA was isolated using the RNeasy Mini Kit (74106, Qiagen), including an on column Dnase digestion (79254, Qiagen), according to the manufacturer's instructions (Rneasy Mini Handbook, Qiagen). Quality and quantity of the total RNA was assessed by the 2100 Bioanalyzer using a Nano chip (Agilent). Total RNA samples having RNA integrity number (RIN) >8 were subjected to library generation. Strand-specific libraries were generated using the TruSeq Stranded mRNA sample preparation kit (Illumina, RS-122-2101/2) according to the manufacturer's instructions (Illumina, document 1000000040498 v.00). In brief, polyadenylated RNA from intact total RNA was purified using oligo-dT beads. Following purification the RNA was fragmented, random primed and reverse transcribed using SuperScript II Reverse Transcriptase (Invitrogen, 18064-014) with the addition of actinomycin D. Second strand synthesis was performed using polymerase I and RnaseH with replacement of dTTP for dUTP. The generated cDNA fragments were 3′ end adenylated and ligated to IDT xGen UDI(10 bp)-UMI(9 bp) paired-end sequencing adapters (Integrated DNA Technologies) and subsequently amplified by 12 cycles of PCR. The libraries were analysed on a 2100 Bioanalyzer using a 7500 chip (Agilent), diluted and pooled equimolar into a multiplex sequencing pool. The libraries were sequenced with 51 paired-end reads on a NovaSeq 6000 using a Reagent Kit v.1.5 (100cycles) (Illumina). After sequencing, data was aligned to the human reference genome Hg38/GRCh38 using HISAT2[54] (v.2.1.0) and the number of reads per gene were calculated using HTSeq count[55] (v.0.5.3). Gene expression differences, between the conditions, were determined using DESeq2[56] (v.1.22.2) with $|\log_2(\text{fold change})| > 1$ and adjusted P value <0.05 cut-offs. Differentially expressed genes were ranked by $\log_2$(fold change expression) and used for gene set enrichment analysis (GSEA) on the Hallmark gene set from msigdbr (v.7.5.1), a previously published GR-activity signature[16] or a newly developed PR-activity signature[17] (Extended Data Table 3), using clusterProfiler[57] (v.3.18.1), (pvalueCutoff = 0.05, pAdjustMethod = "BH"). GSEA enrichment plots have been generated using the plot.gsea function from the Rseb package[48] (v.0.3.2).

Tumour RNA was extracted from FFPE tumour specimens from patients with breast cancer using the MasterPure Complete DNA and RNA Purification Kit (Lucigen, LGC Biosearch Technologies) following the manufacturer's instructions. RNA quality was evaluated using Agilent RNA 6000 Nano Kit (Agilent Technologies) on the Agilent 2100 Bioanalyzer (Agilent Technologies). RNA-seq libraries were prepared using TruSeq Stranded Total RNA Library Prep Gold (20020598, Illumina) according to the manufacturer's protocol and sequenced using 50 bp paired-end sequencing mode on Illumina Novaseq 6000 platform (Illumina). Differential gene expression analysis comparing Post- versus Pre- samples was performed using negative binomial distribution and Benjamini–Hochberg false discovery rate (FDR) with the Bioconductor package DESeq2, applying Wald tests on normalized counts to obtain $\log_2$(fold change) and P values for each gene. To evaluate the activity of pathways of interest (GR-activity signature and PR-activity signature[16,17] (Extended Data Table 3) and Hallmark gene sets) we performed GSEA using the Bioconductor package clusterProfiler. GSEA was performed on genes ranked by the absolute value of $\log_{10}(P \text{ value})$ scaled by the sign of $\log_2$(fold change), tested against gene lists of interest. The enrichment score and NES were computed for each gene set, and nominal P values were estimated by permutation testing. Multiple testing correction was applied using the Benjamini–Hochberg procedure to obtain FDR q values. To estimate the activity of pathways of interest at a single sample level we performed GSVA. Differences in enrichment scores between Post- and Pre- samples were determined by the paired Wilcoxon test. To correlate the activity of GR-activity signature and Hallmark gene sets of interest, their GSVA enrichment scores were correlated through Spearman's linear correlation. All analyses were performed with R studio software (v.2023.03).

Proteomics

For protein digestion, frozen tissues were lysed in boiling guanidine HCl (GuHCl) lysis buffer as previously described[58]. Protein concentration was determined with a Pierce Coomassie (Bradford) Protein Assay Kit (Thermo Scientific), according to the manufacturer's instructions. After dilution to 2 M GuHCl, aliquots corresponding to at least 1.05 mg of protein were digested twice (4 h and overnight) with trypsin (Sigma Aldrich) at 37 °C, enzyme:substrate ratio 1:75. Digestion was quenched by the addition of formic acid (final concentration 5%), after which the peptides were desalted on a Sep-Pak C18 cartridge (Waters). From the eluates, aliquots were collected for proteome analysis, the remainder being reserved for phosphoproteome analysis (not included in this work). Samples were vacuum dried and stored at −80 °C until LC–MS/MS analysis.

Prior to mass spectrometry analysis, the peptides were reconstituted in 2% formic acid. Peptide mixtures were analysed by nano LC–MS/MS on an Orbitrap Exploris 480 Mass Spectrometer equipped with an EASY-NLC 1200 system (Thermo Scientific). Samples were directly loaded onto the analytical column (ReproSil-Pur 120 C18-AQ, 2.4 µm, 75 µm × 500 mm, packed in house). Solvent A was 0.1% formic acid/water and solvent B was 0.1% formic acid/80% acetonitrile. Samples were eluted from the analytical column at a constant flow of 250 nl min^{-1}. For single-run proteome a 90-min gradient was employed containing a 78-min linear increase from 6 to 30% solvent B, followed by a 10-min wash.

Raw data were analysed by DIA-NN (v.1.8)[59] without a spectral library and with 'Deep learning' option enabled. The Swissprot Human database (20,395 entries, release 2021_04) was added for the library-free search. The Quantification strategy was set to Robust LC (high accuracy) and MBR option was enabled. The other settings were kept at the default values. The protein groups report from DIA-NN was used for downstream analysis in Perseus (v.1.6.15.0)[60]. Values were $\log_2$-transformed, after which proteins were filtered for at least 100% valid values in at least one sample group. Missing values were replaced by imputation based on a normal distribution using a width of 0.3 and a minimal downshift of 2.4. Differentially expressed proteins were determined using a Student's t-test (threshold: FDR: 5% and S0: 0.1).

Differentially protein levels were ranked by $\log_2$(fold change) × *P* value and used for GSEA analysis on Hallmarks from the community-contributed functional database from the web-based Gene Set Analysis Toolkit (WebGestalt[61]). GSEA enrichment plots were generated as previously described.

ELISA

Mouse whole blood was collected in Eppendorf tubes. It was allowed to coagulate for 2 h at room temperature, centrifuged for 20 min at 4,000 rpm, then aliquoted into PCR tubes and stored at −80 °C until subsequent use. Whole blood from patients was collected in Vacuette Serum Clot Tubes (BD), centrifuged 20 min at 2,100 rpm then aliquoted into small tubes and stored at −80 °C until use. ELISA assays to detect mouse serum levels of cortisone and progesterone were purchased from R&D System and ALPCO respectively while ELISA assays to detect human serum levels of cortisol and progesterone were purchased from R&D System and Enzo, respectively.

Flow cytometry

Breast cancer nodules were macrodissected from TSAE1-bearing mice and processed to generate single-cell suspensions using the Tumour Dissociation Kit (Miltenyi Biotec, 130-096-730) in conjunction with the gentleMACS Octo Dissociator, following the manufacturers' protocols. The resulting cell suspensions were passed through a 100-µm cell strainer and subsequently washed with fluorescence-activated cell sorting buffer (PBS containing 5% FBS). To ensure the removal of red blood cells, samples were treated with an erythrocyte lysis solution. Following this, samples were pre-incubated with an anti-CD16/CD32 antibody (1:400, 553142, BD Bioscience) and then stained with antibodies specific for extracellular markers, adhering to standard staining protocols. After staining for surface markers, cells were labelled with a live/dead viability dye and subsequently fixed and permeabilized using a fixation/permeabilization solution (eBioscience, Invitrogen) for intracellular staining. All antibodies utilized for flow cytometry were titrated to account for lot-dependent variations, as described in Extended Data Fig. 7f. Immune cell populations were classified as follows: lymphoid cells ($CD45^+CD11b^-$), myeloid cells ($CD45^+CD11b^+$), neutrophils ($CD45^+CD11b^+Ly6G^+$), non-classical monocytes ($CD45^+CD11b^+Ly6G^-Ly6C^-$) and dendritic cells ($CD45^+F4/80^-CD11c^{hi}MHCII^{hi}$) (for gating strategy used, see Supplementary Fig. 1). Sample acquisition was performed using a five-laser Aurora spectral flow cytometer (Cytek Biosciences), and data analysis was conducted using FlowJo v.10 software.

Statistical analysis

Statistical analyses were performed using GraphPad Prism software v.10.4.1 (GraphPad Software) or in R v.4.0.2 (R Core Team 2020, https://www.R-project.org). Paired *t*-test or one-way analysis of variance (ANOVA) was used to calculate changes in the majority of the analyses (unless otherwise stated) and only *P* values <0.05 were considered significant. Two-tailed Wilcoxon signed rank test was used to compare cortisol plasmatic concentration measured before FMD (Pre-FMD) and after FMD (Post-FMD). For the animal experiments, a linear mixed-effects model was utilized to assess whether the mass volume exhibits a statistically significant trend relative to the treatment over time. The model was constructed using the two-way ANOVA or mixed-effect model (in case of missing data) from GraphPad Prism software v.10.4.1. The fixed-effects model matrix was generated by the interaction of time (measured in days after injection) and treatment. The random-effects term was specified as the interaction between the treatment group and the blocking factor of the mouse ID. Subsequent pairwise post hoc multiple comparisons were conducted using the same software. Statistical significance was determined by *P* values less than 0.05. Linear mixed-effect model results are presented in the Supplementary Information.

Reporting summary

Further information on research design is available in the Nature Portfolio Reporting Summary linked to this article.

Data availability

All mouse data generated or analysed during this study are included in this published article (and its supplementary information files). The ChIP–seq and RNA-seq data relative to mice xenografts have been deposited to the GEO database (GSE260486). The ChIP–seq pipeline is publically accessible[62]. RNA-seq data for patients with breast cancer are deposited on the European Genome-Phenome Archive (EGA) under accession number EGAS00001004944. The mass spectrometry proteomics data have been deposited to the ProteomeXchange Consortium via the PRIDE[63] partner repository with the dataset identifier PXD049477. Source data are provided with this paper.

39. Behbod, F. et al. An intraductal human-in-mouse transplantation model mimics the subtypes of ductal carcinoma in situ. *Breast Cancer Res.* **11**, R66 (2009).
40. Lee, C. et al. Fasting cycles retard growth of tumors and sensitize a range of cancer cell types to chemotherapy. *Sci. Transl. Med.* **4**, 124ra127 (2012).
41. Zhang, J. et al. Administration of dexamethasone protects mice against ischemia/reperfusion induced renal injury by suppressing PI3K/AKT signaling. *Int. J. Clin. Exp. Pathol.* **6**, 2366–2375 (2013).
42. Lutz, C. et al. Large-scale characterization of orthotopic cell line-derived xenografts identifies TGF-β signaling as a key regulator of breast cancer morphology and aggressiveness. *Cancer Res.* **85**, 2608–2625 (2025).
43. Arends, J. et al. ESPEN expert group recommendations for action against cancer-related malnutrition. *Clin. Nutr.* **36**, 1187–1196 (2017).
44. Reidy, P. T. et al. Protein blend ingestion following resistance exercise promotes human muscle protein synthesis. *J. Nutr.* **143**, 410–416 (2013).
45. Singh, A. A. et al. Optimized ChIP-seq method facilitates transcription factor profiling in human tumors. *Life Sci. Alliance* **2**, e201800115 (2019).
46. Li, H. & Durbin, R. Fast and accurate short read alignment with Burrows–Wheeler transform. *Bioinformatics* **25**, 1754–1760 (2009).
47. Ramírez, F. et al. deepTools2: a next generation web server for deep-sequencing data analysis. *Nucleic Acids Res.* **44**, W160–W165 (2016).
48. Gregoricchio, S. et al. HDAC1 and PRC2 mediate combinatorial control in SPI1/PU.1-dependent gene repression in murine erythroleukaemia. *Nucleic Acids Res.* **50**, 7938–7958 (2022).
49. Ross-Innes, C. S. et al. Differential oestrogen receptor binding is associated with clinical outcome in breast cancer. *Nature* **481**, 389–393 (2012).
50. Yu, G., Wang, L.-G. & He, Q.-Y. ChIPseeker: an R/Bioconductor package for ChIP peak annotation, comparison and visualization. *Bioinformatics* **31**, 2382–2383 (2015).
51. Layer, R. M. et al. GIGGLE: a search engine for large-scale integrated genome analysis. *Nat. Methods* **15**, 123–126 (2018).
52. Sanjana, N. E., Shalem, O. & Zhang, F. Improved vectors and genome-wide libraries for CRISPR screening. *Nat. Methods* **11**, 783–784 (2014).
53. Bankhead, P. et al. QuPath: Open source software for digital pathology image analysis. *Sci. Rep.* **7**, 16878 (2017).
54. Kim, D., Paggi, J. M., Park, C., Bennett, C. & Salzberg, S. L. Graph-based genome alignment and genotyping with HISAT2 and HISAT-genotype. *Nat. Biotechnol.* **37**, 907–915 (2019).
55. Anders, S., Pyl, P. T. & Huber, W. HTSeq–a Python framework to work with high-throughput sequencing data. *Bioinformatics* **31**, 166–169 (2015).
56. Love, M. I., Huber, W. & Anders, S. Moderated estimation of fold change and dispersion for RNA-seq data with DESeq2. *Genome Biol.* **15**, 550 (2014).
57. Yu, G., Wang, L. G., Han, Y. & He, Q. Y. clusterProfiler: an R package for comparing biological themes among gene clusters. *Omics* **16**, 284–287 (2012).
58. Jersie-Christensen, R. R., Sultan, A. & Olsen, J. V. Simple and reproducible sample preparation for single-shot phosphoproteomics with high sensitivity. *Methods Mol. Biol.* **1355**, 251–260 (2016).
59. Demichev, V., Messner, C. B., Vernardis, S. I., Lilley, K. S. & Ralser, M. DIA-NN: neural networks and interference correction enable deep proteome coverage in high throughput. *Nat. Methods* **17**, 41–44 (2020).
60. Tyanova, S. et al. The Perseus computational platform for comprehensive analysis of (prote)omics data. *Nat. Methods* **13**, 731–740 (2016).
61. Elizarraras, J. M. et al. WebGestalt 2024: faster gene set analysis and new support for metabolomics and multi-omics. *Nucleic Acids Res.* **52**, W415–W421 (2024).
62. Gregoricchio, S. sebastian-gregoricchio/SPACCa: v0.1.0 (0.1.0). *Zenodo* https://doi.org/10.5281/zenodo.15309654 (2025).
63. Deutsch, E. W. et al. The ProteomeXchange consortium at 10 years: 2023 update. *Nucleic Acids Res.* **51**, D1539–D1548 (2023).

Acknowledgements We thank S. Prekovic and the members of the Zwart/Bergman and Nencioni laboratories for valuable feedback, suggestions and input throughout the project. We acknowledge the NKI Animal facility and pathology for all the support with mouse experiments, NKI genomics core facility for the next generation sequencing and bioinformatics support, the NKI Proteomics/Mass Spectometry Facility for the proteomic and bioinformatics analyses, and

the NKI-AVL Core Facility Molecular Pathology and Biobanking (CFMPB) for supplying NKI-AVL Biobank material and/or lab support. W.Z. is further supported by Dutch Cancer Society, Alpe d'HuZes and a VIDI grant (9171640) from the Netherlands Organization for Scientific Research (NWO). This work was supported in part by the Associazione Italiana per la Ricerca sul Cancro (AIRC; 22098 to A.N. and MFAG 26482 to I.C.).

Author contributions N.P. and W.Z. conceived the study. N.P. and I.C. performed most of the experiments. N.P., T.M.S., S.G. and F.L. performed the computational and statistical analyses. I.C., A.G., C.L. and S.H. performed the in vivo experiments. D.T. performed the FACS experiments and analysis. M.R. produced and provided the GR-KO cells. J.S. and J.-Y.S. performed the pathological analyses. S.P.-O. performed the immunohistochemistry quantifications. F.L., C.V., F.d.B., A.N., I.C. and A.P. were involved in the clinical trials and translational analyses in patient samples. M.D.C., H.H., L.P., L.A., J.J., A.N., I.C. and W.Z. contributed to the study design and supervision. N.P., I.C., A.N. and W.Z. wrote the manuscript with input of all authors. All authors evaluated the results and edited the manuscript.

Competing interests A.N. and I.C. hold intellectual property rights on clinical uses of FMDs. C.V. and F.d.B. hold intellectual property rights on clinical uses of FMDs. F.L. reports honoraria as a speaker from Novartis, Pfizer and Accademia Nazionale di Medicina. C.V. and F.d.B. report roles in advisory boards, consultancy activity or having received honoraria as speakers from Pfizer, Novartis, Eli Lilly, Astra Zeneca, Daiichi Sankyo, Menarini Stemline, Gilead, MSD and Istituto Gentili. The other authors declare no competing interests.

Additional information

Supplementary information The online version contains supplementary material available at https://doi.org/10.1038/s41586-025-09869-0.

Correspondence and requests for materials should be addressed to Irene Caffa or Wilbert Zwart.

Peer review information *Nature* thanks Marcus Goncalves, Stephen Hursting and Eneda Toska for their contribution to the peer review of this work. Peer review reports are available.

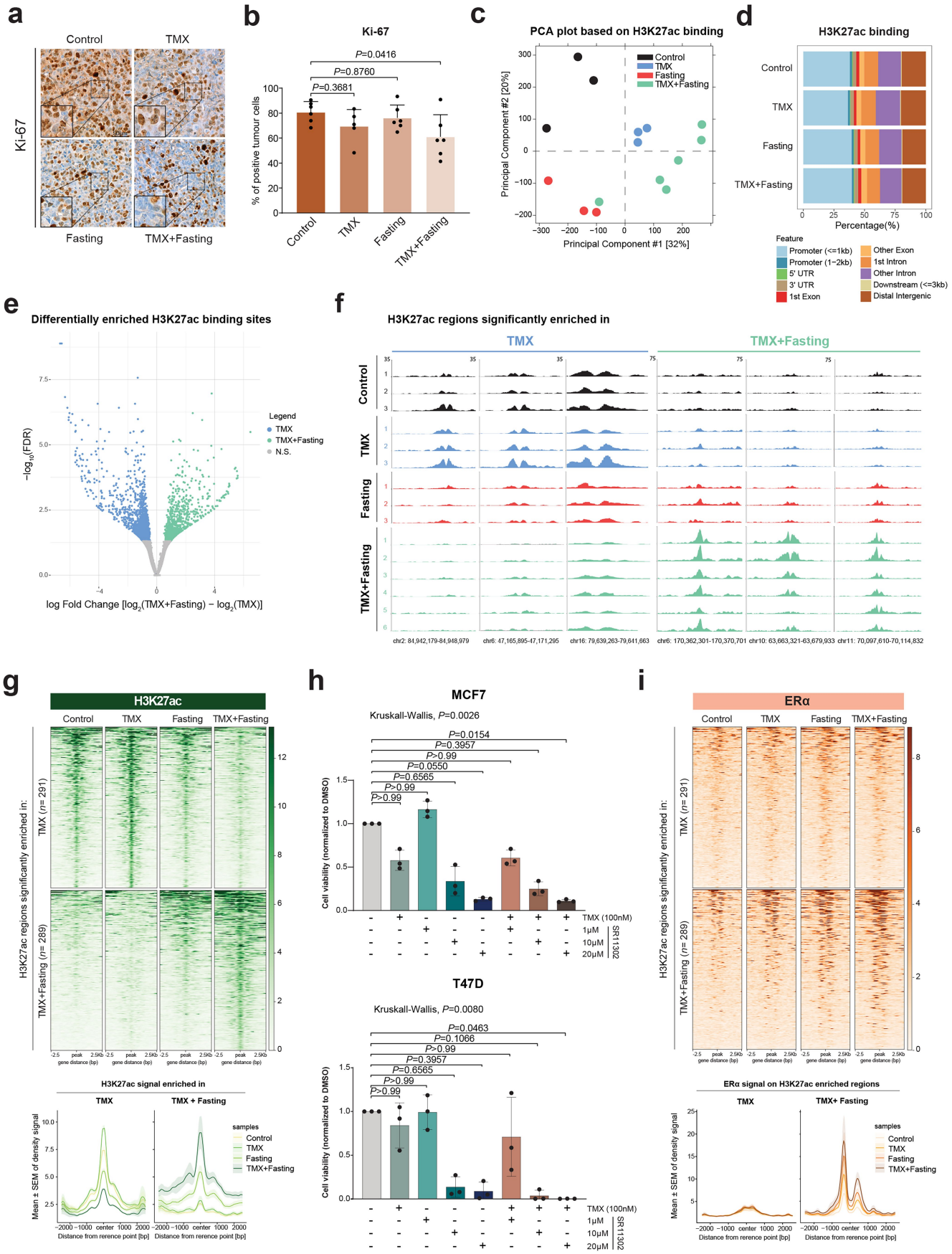

Extended Data Fig. 1 | See next page for caption.

Extended Data Fig. 1 | Fasting reduces tumour growth and exerts epigenetic changes in ERα+ xenografts. a. Representative immunohistochemistry stainings for Ki-67 in MCF7 xenografts from mice treated with *ad-libitum* diet (control, $n = 6$), tamoxifen (TMX, $n = 5$), fasting ($n = 6$) and combination (TMX+Fasting, $n = 6$). n, represents different tumour samples analysed. **b**. Percentage of tumour cells stained for Ki-67 in the different depicted conditions. Data are presented as mean ± SD. *P*-values represents one-way ANOVA with Dunnet's multiple test correction. **c**. PCA plot on H3K27ac ChIP-seq data, for all 4 conditions. **d**. Genomic distribution of the H3K27ac ChIP-seq peaks for all 4 conditions. **e**. Volcano plot of the differentially-enriched H3K27ac sites between TMX and TMX+Fasting. **f**. H3K27ac ChIP-seq data for all 4 conditions, depicting representative regions that are differentially-enriched between TMX and TMX+Fasting. The genomic coordinates are annotated. **g**. Heat map showing H3K27ac ChIP-seq signal for all 4 conditions at differentially-enriched H3K27ac regions in comparing TMX or TMX+Fasting treated xenografts (top). Regions were sorted on H3K27ac signal intensity. Data are centred at H3K27ac peak, within a ± 2.5 kb window. Average density plots for ChIP-seq signal for H3K27ac in xenografts treated with the respective conditions (bottom). Data are presented as mean values ± SEM. **h**. Cell viability of MCF7 and T47D cells treated with tamoxifen and increased concentrations of AP-1 inhibitor SR11302, alone or in combination. Data are from three biological replicates and are presented as mean ± SD. *P*-values represents Kruskal-Wallis followed by Dunn post-hoc correction. **i**. Heat map depicting ERα ChIP-seq signal for all 4 conditions at differentially-enriched H3K27ac regions, comparing TMX *versus* TMX+Fasting treated xenografts (top). Regions were sorted on ERα signal. Data are centred on the ERα peak, within a ± 2.5 kb window. Average density plots are shown for ChIP-seq signal for ERα in MCF7 xenografts treated with the respective conditions (bottom). Data are presented as mean values ± SEM.

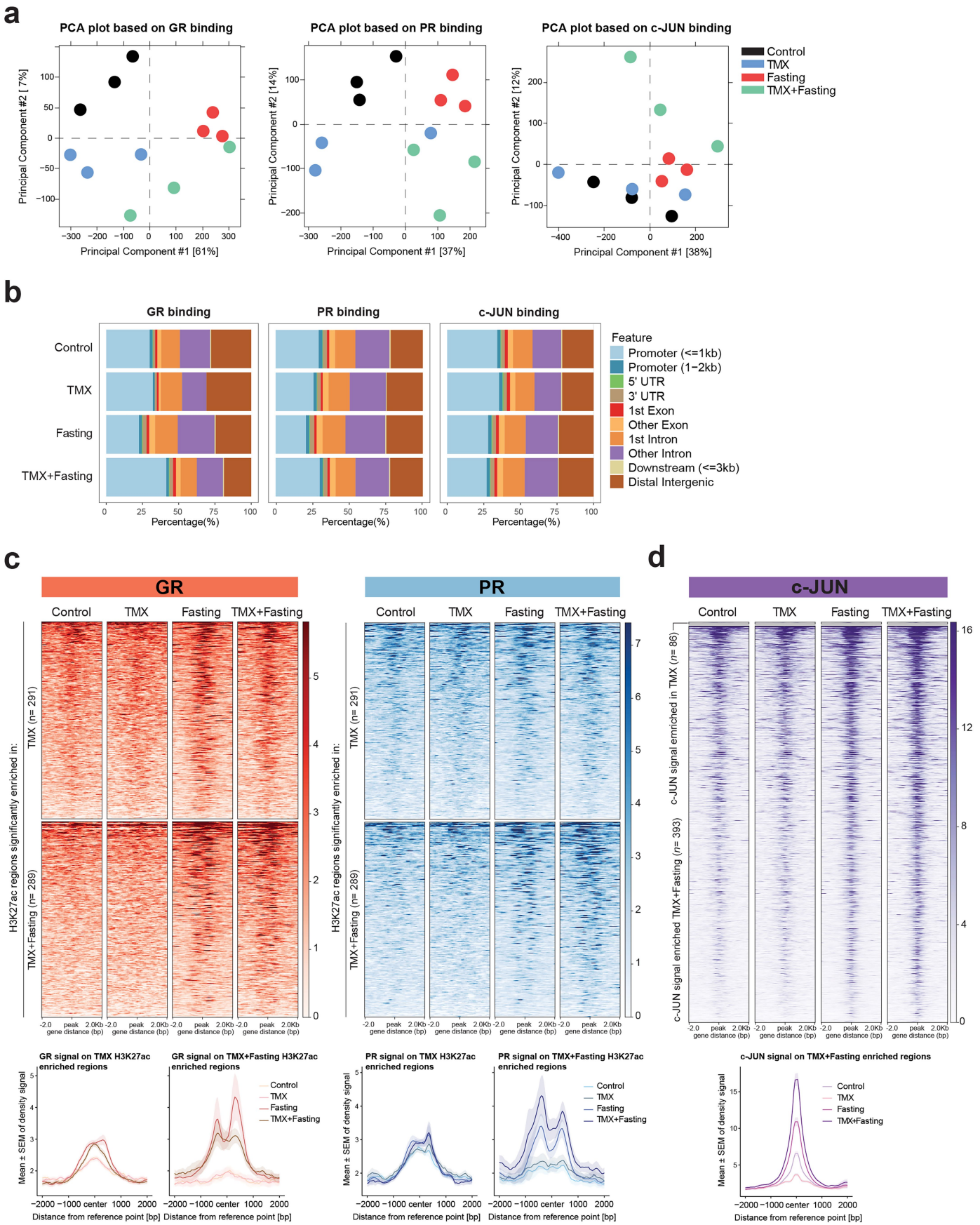

Extended Data Fig. 2 | See next page for caption.

Extended Data Fig. 2 | GR and PR chromatin binding is induced by fasting treatment. a. PCA plots for GR, PR and c-JUN ChIP-seq regions between the 4 conditions in MCF7 xenografts. **b**. Genomic distribution of GR, PR and c-JUN ChIP-seq regions between the 4 conditions. **c**. Heat map of GR and PR ChIP-seq signal for all 4 conditions, at differentially-enriched H3K27ac sites between TMX and TMX+Fasting (top). Regions were sorted on H3K27ac signal. Data are centred at H3K27ac peak, within a ± 2 kb window. Average density plots is shown for ChIP-seq signal of GR and PR in xenografts for all 4 treatment conditions (bottom). Data are presented as mean values ± SEM. **d**. Heat map depicting ChIP-seq signal for c-JUN in MCF7 xenografts for all 4 treatment conditions, visualizing differentially-enriched c-JUN sites, comparing TMX and TMX+Fasting regions (top). Regions were sorted according to decreasing c-JUN signal. Data are centred at c-JUN peak, within a ± 2 kb window. Average density plots is shown for c-JUN ChIP-seq signal for all 4 conditions in TMX+Fasting enriched regions (bottom). Data are presented as mean values ± SEM.

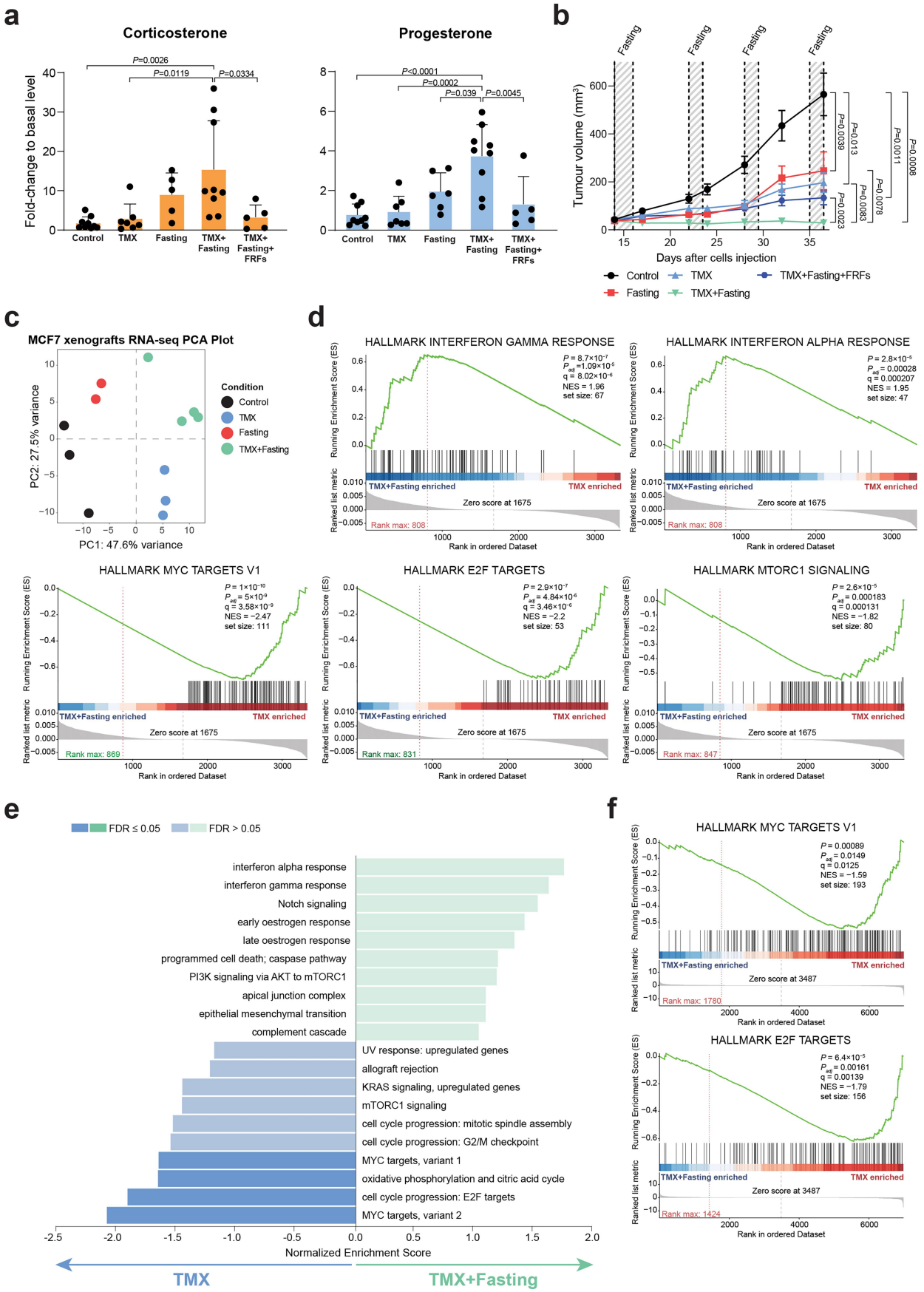

Extended Data Fig. 3 | See next page for caption.

Extended Data Fig. 3 | Tumour growth and systemic effects of fasting-reduced factors treatment and differential transcriptional activity between xenografts treated with tamoxifen alone or combined with fasting. a. Fold-change to baseline levels of corticosterone and progesterone levels on mice blood after 4 cycles of all treatment conditions. Data are shown as mean ± SD and analysed by one-way ANOVA followed by Tukey's multiple comparison test. **b**. MCF7 xenograft tumour growth in six/eight-week-old female athymic nude mice in the different treatment arms. Control $n = 14$, TMX $n = 12$, Fasting $n = 15$, TMX+Fasting $n = 12$, TMX+Fasting+FRFs $n = 7$. n, number of tumours per treatment group. Data are shown as mean ± SEM and P-values are determined by mixed effect model with Tukey's multiple test correction (see Supplementary File 1) and two-tailed Student's t-test (P-values of last day are represented). **c**. PCA plot based on gene expression data between MCF7 xenografts for all treatment conditions. **d**. Enrichment plots of the differentially enriched Hallmarks performed on transcriptomic data comparing TMX (top) and TMX+Fasting (bottom) xenografts. NES is calculated by weighted Kolmogorov-Smirnov test and P-value determined by permutation-based testing with multiple Benjamini-Hochberg (BH) hypothesis correction. **e**. GSEA for Hallmark gene sets performed on bulk proteomic data from xenografts treated with TMX alone or TMX+Fasting. **f**. Representative enrichment plots of the two top-differentially enriched Hallmarks performed on bulk proteomic data, when comparing TMX-enriched *vs* TMX+Fasting-enriched pathways. NES is calculated by weighted Kolmogorov-Smirnov test and P-value determined by permutation-based testing with multiple Benjamini-Hochberg (BH) hypothesis correction.

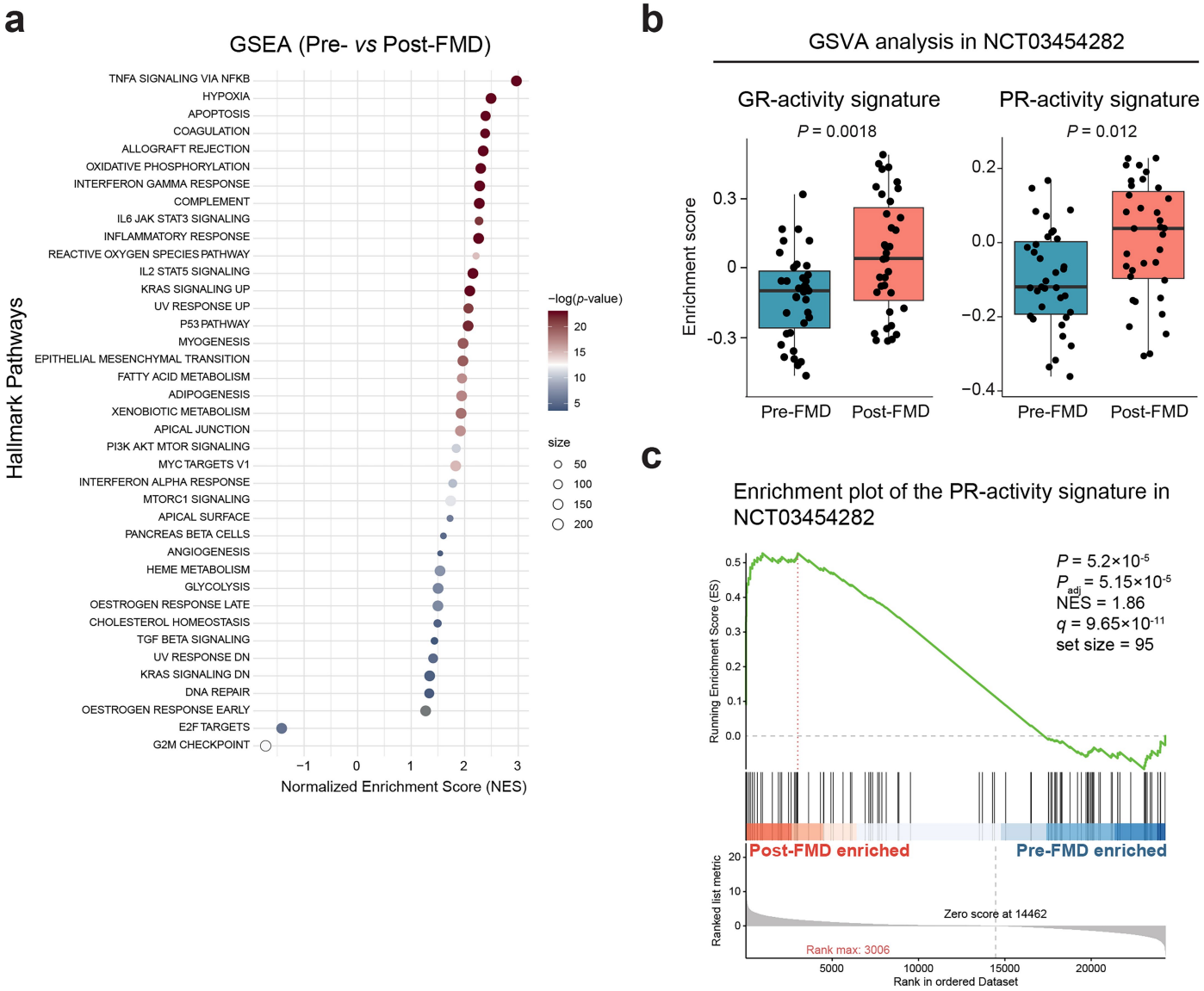

Extended Data Fig. 4 | Transcriptomic analyses of BC patients treated with 5 days FMD diet. a. Gene set enrichment analysis for Hallmarks pathways. Differentially-enriched pathways between pre- and post-5 days FMD in BC patients are shown. NES is calculated by weighted Kolmogorov-Smirnov test and *P*-value determined by permutation-based testing with multiple Benjamini-Hochberg (BH) hypothesis correction. **b.** GSVA enrichment scores of the GR- and PR-activity signature in transcriptomic matched samples from BC patients pre-and post-5 days of FMD. Each boxplot indicates the 25th and 75th percentiles of the distribution of GSVA ESs, while the horizontal line inside the box indicates the median value of the distribution. Dots indicate measurements in individual patients. *P*-values refer to the two-sided paired Wilcoxon test. **c.** Enrichment plot for PR-activity signature in matched tumour samples of BC patients Pre- and Post- 5 days FMD. NES and *P*-values are depicted. NES is calculated by weighted Kolmogorov-Smirnov test and *P*-value determined by permutation-based testing with multiple Benjamini-Hochberg (BH) hypothesis correction.

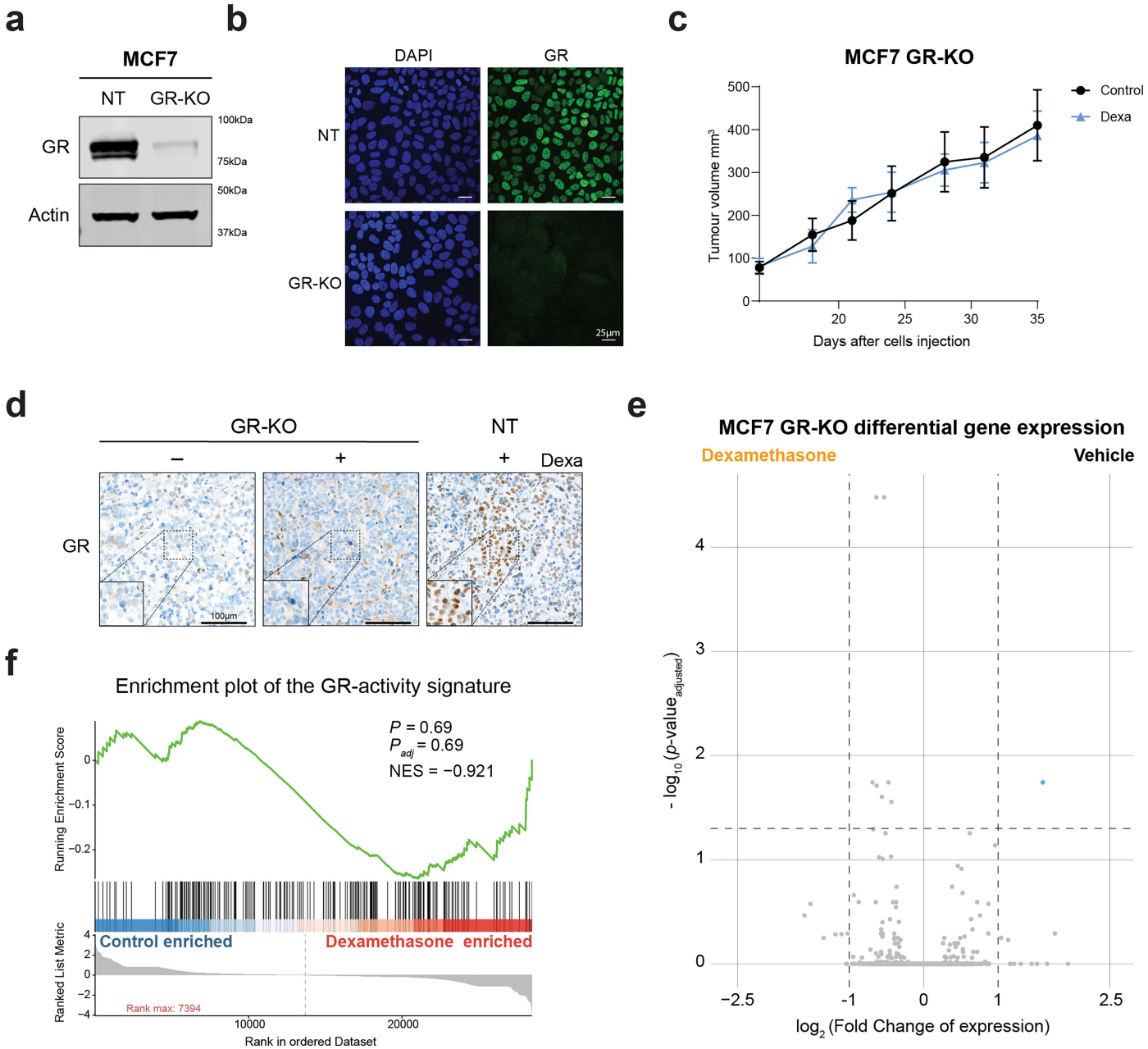

Extended Data Fig. 5 | GR-KO MCF7 xenografts generation and response to dexamethasone treatment, in vivo. a. Western blot for GR in NT (non-targeting) and GR-KO MCF7 cells; Actin was used as loading control. Three biological replicates were performed ($n = 3$). For gel source data, see Supplementary Fig. 1. **b.** Immunofluorescence for DAPI and GR in NT and GR-KO MCF7 cells. Two biological replicates were performed ($n = 2$). **c.** Xenograft MCF7 GR-KO tumour volume in six/eight-week-old female athymic nude mice treated with vehicle or Dexa. Data are shown as mean ± SEM. Control $n = 6$, Dexa $n = 5$. n, number of tumours per treatment group. **d.** Representative IHC images for GR in MCF7 GR-KO and NT xenografts treated with vehicle or Dexa. GR-KO control $n = 5$, GR-KO dexa $n = 4$, NT $n = 3$. n, number of tumours analysed. **e.** Volcano plot of the differentially expressed transcripts between vehicle and Dexa treated MCF7 GR-KO xenografts. Differential gene expression was determined by two-sided Wald test. **f.** Enrichment plot of a pan-cancer GR-activity signature for the depicted conditions. NES is calculated by weighted Kolmogorov-Smirnov test and P-value determined by permutation-based testing with multiple Benjamini-Hochberg (BH) hypothesis correction.

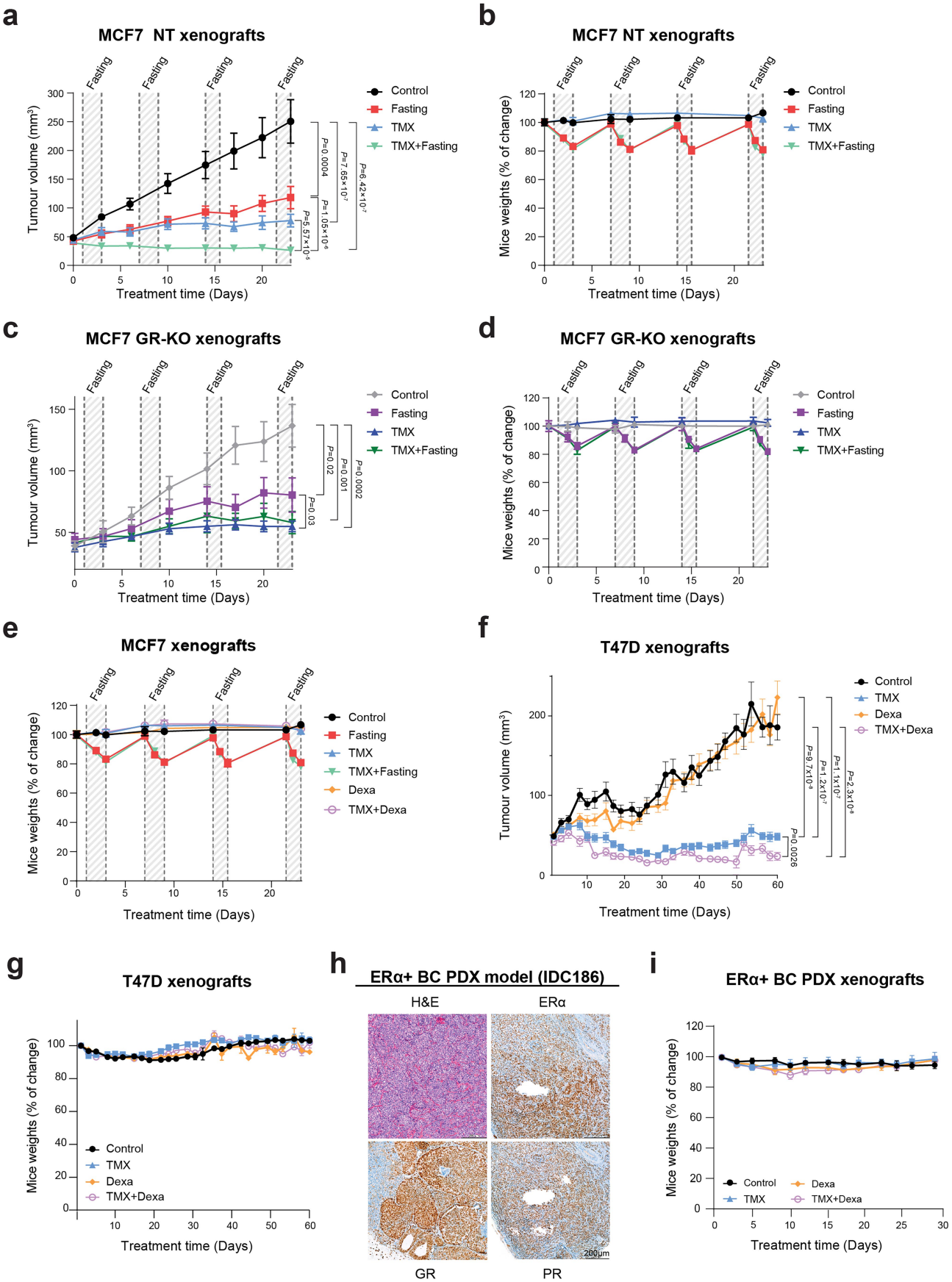

Extended Data Fig. 6 | See next page for caption.

Extended Data Fig. 6 | Tumour outgrowth and body weight analyses for respective xenografts under all treatment conditions. a. MCF7 NT xenografts tumour growth in six-eight-week old female athymic nude mice treated with the respective depicted conditions (Control $n = 8$, TMX $n = 9$, Fasting $n = 8$, TMX+Fasting $n = 11$). n, number of tumours analysed. Data are shown as mean ± SEM and P-values are determined by mixed effect model with Tukey's multiple test correction (see Supplementary File 1) and two-tailed Student's t-test (P-values of last day are represented). **b**. Body weight changes (%) in mice during the 4 treatment cycle from the experiment performed in a. Data are shown as mean ± SD. Control $n = 4$, TMX $n = 5$, Fasting $n = 5$, TMX+Fasting $n = 6$. n, number of mice analysed. **c**. MCF7 GR-KO xenografts tumour growth in six-eight-week old female athymic nude mice treated with the respective depicted conditions (Control $n = 7$, TMX $n = 7$, Fasting $n = 6$, TMX+Fasting $n = 9$). n, number of tumours analysed. Data are shown as mean ± SEM and P-values are determined by mixed effect model with Tukey's multiple test correction (see Supplementary File 1) and two-tailed Student's t-test (P-values of last day are represented). **d**. Body weight changes (%) in mice during the 4 cycle treatments from the experiment performed in c. Data are shown as mean ± SD. Control $n = 4$, TMX $n = 4$, Fasting $n = 4$, TMX+Fasting $n = 6$. n, number of mice analysed. **e**. Body weight changes (%) in mice during 4 weeks of depicted treatments from Fig. 4f. Data are shown as mean ± SD. Control $n = 4$, TMX $n = 5$, Fasting $n = 5$, TMX+Fasting $n = 6$, Dexa $n = 4$, TMX+Dexa $n = 4$. n, number of mice analysed. **f**. T47D xenograft tumour outgrowth in six-eight-week old female NSG mice in the different treatment arms (Control $n = 16$; TMX $n = 16$; Dexa $n = 19$ and TMX+Dexa $n = 13$). n, number of tumours analysed. Data are shown as mean ± SEM and P-values are determined by mixed effect model with Tukey's multiple test correction (see Supplementary File 1) and two-tailed Student's t-test (P-values of last day are represented). **g**. Body weight changes (%) in mice during 7 weeks of depicted treatments from f. Data are shown as mean ± SD. (Control $n = 8$; TMX $n = 8$; Dexa $n = 9$ and TMX+Dexa $n = 7$). n, number of mice analysed. **h**. Representative immunohistochemistry stainings for H&E, ERα ($n = 3$), GR ($n = 1$) and PR ($n = 3$) in the IDC186 PDX model. n, number of independent tumour samples. **i**. Body weight changes (%) in mice during 4 weeks of depicted treatments from Fig. 4e. Data are shown as mean ± SD.

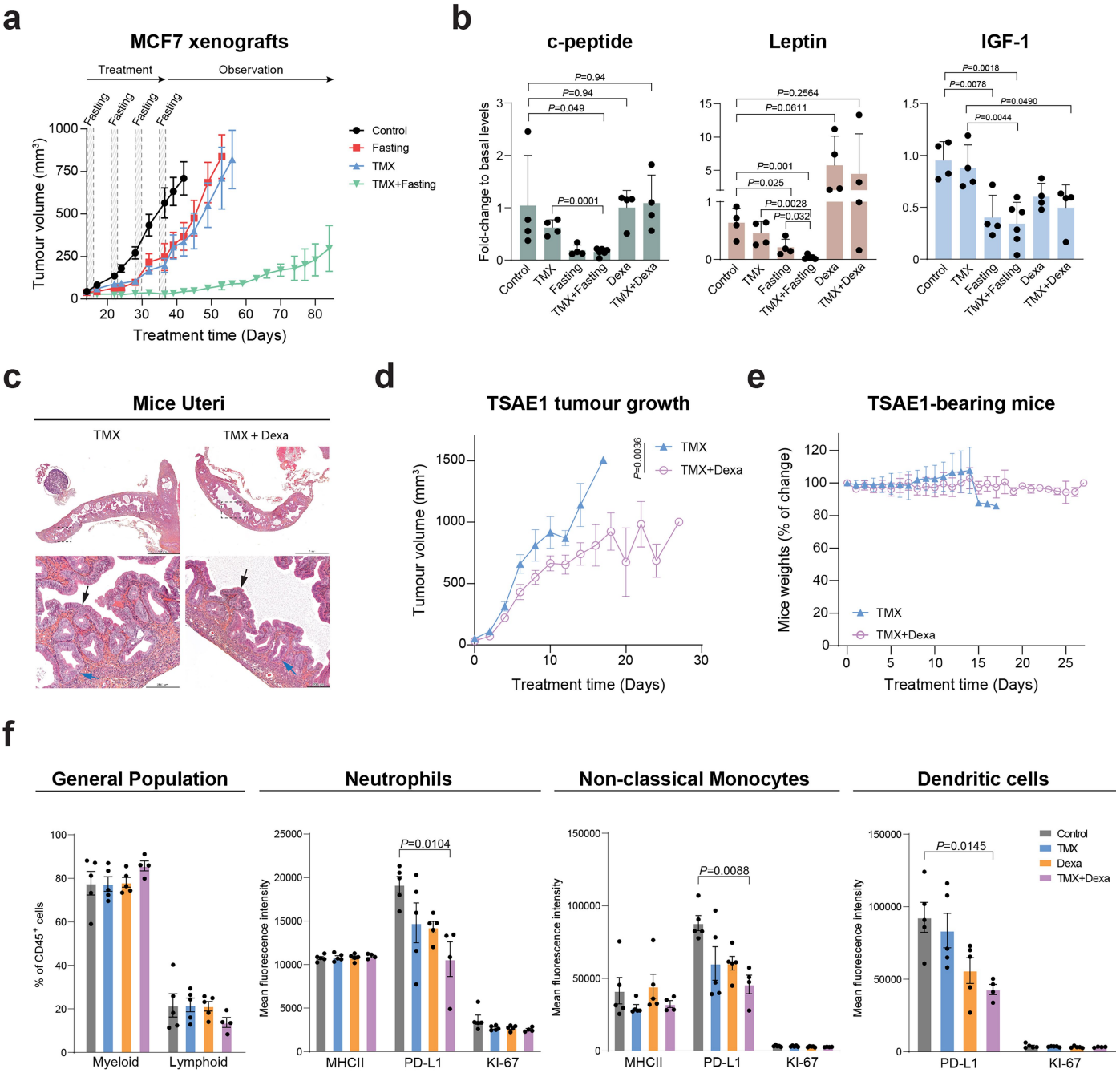

Extended Data Fig. 7 | Effects of Dexa treatment in circulating FRFs, TMX-induced uteri hyperplasia and PD-L1 expression levels in several immune-populations. a. MCF7 xenografts tumours volume in six-eight-week old female athymic nude mice treated with the depicted conditions (Control $n = 7$; TMX $n = 7$, Fasting $n = 8$; TMX+Fasting $n = 8$). After one month, all treatments were stopped and tumours were allowed to grow. Data are shown as mean ± SEM. **b**. Fold-change differences to basal conditions of circulating c-peptide, leptin and IGF-1 (FRFs) levels in in six-eight-week old female athymic nude mice xenografted with MCF7 cells, treated with the respective depicted conditions. Control $n = 4$, TMX $n = 4$, Fasting $n = 4$, TMX+Fasting $n = 6$, Dexa $n = 4$, TMX+Dexa $n = 4$. n, number of mice per treatment group. Data are shown as mean ± SD and analysed by two-tailed Student t-test. **c**. Microphotographs of H&E staining of mouse uteri after TMX (left panel) and TMX + Dexa (right panel) treatments. Black arrows indicate luminal epithelia and blue arrows indicate glandular epithelia from the endometrium. TMX $n = 9$, TMX+Dexa $n = 8$. n, represents different mice uteri analysed. **d**. TSAE1-engrafted tumour growth in immune-competent mice treated with either TMX alone ($n = 17$) or combined with Dexa ($n = 19$) for up to 26 days. n, number of tumours analysed. Data are shown as mean ± SEM and P-value is determined by mixed effect model. **e**. Body weight changes (%) in mice during the cycle treatments from the experiment performed in e. Data are shown as mean ± SD. TMX $n = 10$, TMX+Dexa $n = 10$. n, number of mice analysed. **f**. Bar plots showing the mean fluorescence intensity for selected markers for systemic myeloid cells and lymphoid cells (CD45 + CD11b+ and CD45 + CD11b- respectively), neutrophils (CD45 + CD11b + Ly6G +), non-classical monocytes (CD45 + CD11b + Ly6G- Ly6C-) and dendritic cells (CD45 + F4/80- CD11c high MHCII high) from TSAE1-bearing mice treated with three rounds of control treatment, TMX, Dexa, or TMX+Dexa (7 days). Control $n = 5$, TMX $n = 5$, Dexa $n = 5$, TMX+Dexa $n = 4$. n, number of mice per treatment group. Data are shown as mean ± SD. Statistical significance was determined by one-way ANOVA with Tukey's multiple comparison test.

Extended Data Table 1 | ChIP-seq analysis quality controls

ChIP-seq quality controls

sample	n_peaks	FRiP	M_reads_mapped
MCF7 xenograft_control (no treatments)_Replicate 1_ER	29741	0.078	61.5
MCF7 xenograft_control (no treatments)_Replicate 2_ER	33150	0.095	49.7
MCF7 xenograft_control (no treatments)_Replicate 3_ER	13670	0.039	55.6
MCF7 xenograft_Tamoxifen treated_Replicate 1_ER	47243	0.138	62.3
MCF7 xenograft_Tamoxifen treated_Replicate 2_ER	9365	0.022	58.1
MCF7 xenograft_Tamoxifen treated_Replicate 3_ER	34206	0.098	53.1
MCF7 xenograft_ Fasting_Replicate 1_ER	46901	0.147	56.0
MCF7 xenograft_ Fasting_Replicate 2_ER	47993	0.148	76.2
MCF7 xenograft_ Fasting_Replicate 3_ER	37040	0.102	70.4
MCF7 xenograft_ Fasting + Tamoxifen_Replicate 1_ER	72054	0.257	67.0
MCF7 xenograft_ Fasting + Tamoxifen_Replicate 2_ER	49417	0.156	61.8
MCF7 xenograft_ Fasting + Tamoxifen_Replicate 3_ER	61939	0.203	64.2
MCF7 xenograft_ Fasting + Tamoxifen_Replicate 4_ER	40273	0.147	48.8
MCF7 xenograft_ Fasting + Tamoxifen_Replicate 5_ER	711	0.003	38.2
MCF7 xenograft_ Fasting + Tamoxifen_Replicate 6_ER	25818	0.087	35.0
MCF7 xenograft_control (no treatments)_Replicate 1_H3K27ac	57810	0.538	43.2
MCF7 xenograft_control (no treatments)_Replicate 2_H3K27ac	49081	0.636	51.7
MCF7 xenograft_control (no treatments)_Replicate 3_H3K27ac	57808	0.604	66.2
MCF7 xenograft_Tamoxifen treated_Replicate 1_H3K27ac	53674	0.675	68.2
MCF7 xenograft_Tamoxifen treated_Replicate 2_H3K27ac	63146	0.562	59.7
MCF7 xenograft_Tamoxifen treated_Replicate 3_H3K27ac	61864	0.588	70.1
MCF7 xenograft_ Fasting_Replicate 1_H3K27ac	60350	0.568	55.1
MCF7 xenograft_ Fasting_Replicate 2_H3K27ac	62978	0.571	67.8
MCF7 xenograft_ Fasting_Replicate 3_H3K27ac	59070	0.538	52.7
MCF7 xenograft_ Fasting + Tamoxifen_Replicate 1_H3K27ac	52298	0.634	59.9
MCF7 xenograft_ Fasting + Tamoxifen_Replicate 2_H3K27ac	57696	0.579	58.9
MCF7 xenograft_ Fasting + Tamoxifen_Replicate 3_H3K27ac	54060	0.587	67.9
MCF7 xenograft_ Fasting + Tamoxifen_Replicate 4_H3K27ac	62138	0.594	61.1
MCF7 xenograft_ Fasting + Tamoxifen_Replicate 5_H3K27ac	69495	0.414	49.8
MCF7 xenograft_ Fasting + Tamoxifen_Replicate 6_H3K27ac	63469	0.498	55.5
MCF7 xenograft_control (no treatments)_Replicate 1_GR	6514	0.007	35.6
MCF7 xenograft_control (no treatments)_Replicate 2_GR	5452	0.015	34
MCF7 xenograft_control (no treatments)_Replicate 3_GR	357	0.051	42.8
MCF7 xenograft_Tamoxifen treated_Replicate 1_GR	820	0.003	37.9
MCF7 xenograft_Tamoxifen treated_Replicate 2_GR	3944	0.007	36.8
MCF7 xenograft_Tamoxifen treated_Replicate 3_GR	1312	0.002	24.7
MCF7 xenograft_ Fasting_Replicate 1_GR	16421	0.039	46.7
MCF7 xenograft_ Fasting_Replicate 2_GR	22725	0.059	39.1
MCF7 xenograft_ Fasting_Replicate 3_GR	21758	0.053	51.8
MCF7 xenograft_ Fasting+Tamoxifen_Replicate 1_GR	9669	0.02	29.9
MCF7 xenograft_ Fasting+Tamoxifen_Replicate 2_GR	33000	0.099	41.1
MCF7 xenograft_ Fasting+Tamoxifen_Replicate 3_GR	2447	0.005	34
MCF7 xenograft_control (no treatments)_Replicate 1_c-JUN	44567	0.078	23.9
MCF7 xenograft_control (no treatments)_Replicate 2_c-JUN	44402	0.135	34.3
MCF7 xenograft_control (no treatments)_Replicate 3_c-JUN	12203	0.087	36.2
MCF7 xenograft_Tamoxifen treated_Replicate 1_c-JUN	9248	0.017	34.5
MCF7 xenograft_Tamoxifen treated_Replicate 2_c-JUN	42874	0.145	30.7
MCF7 xenograft_Tamoxifen treated_Replicate 3_c-JUN	49230	0.088	24.5
MCF7 xenograft_ Fasting_Replicate 1_c-JUN	28022	0.087	39.1
MCF7 xenograft_ Fasting_Replicate 2_c-JUN	36738	0.131	36.6
MCF7 xenograft_ Fasting_Replicate 3_c-JUN	30904	0.096	22.4
MCF7 xenograft_ Fasting+Tamoxifen_Replicate 1_c-JUN	32444	0.067	20.1
MCF7 xenograft_ Fasting+Tamoxifen_Replicate 2_c-JUN	50206	0.208	36.3
MCF7 xenograft_ Fasting+Tamoxifen_Replicate 3_c-JUN	33115	0.084	33.6
MCF7 xenograft_control (no treatments)_Replicate 1_PR	10825	0.019	35.1
MCF7 xenograft_control (no treatments)_Replicate 2_PR	21080	0.043	37.2
MCF7 xenograft_control (no treatments)_Replicate 3_PR	14426	0.033	43.6
MCF7 xenograft_Tamoxifen treated_Replicate 1_PR	5939	0.011	31.7
MCF7 xenograft_Tamoxifen treated_Replicate 2_PR	27179	0.056	38.8
MCF7 xenograft_Tamoxifen treated_Replicate 3_PR	4298	0.008	27.9
MCF7 xenograft_ Fasting_Replicate 1_PR	26274	0.055	53.3
MCF7 xenograft_ Fasting_Replicate 2_PR	39145	0.083	52.7
MCF7 xenograft_ Fasting_Replicate 3_PR	29032	0.068	44.9
MCF7 xenograft_ Fasting+Tamoxifen_Replicate 1_PR	21180	0.06	23.9
MCF7 xenograft_ Fasting+Tamoxifen_Replicate 2_PR	50226	0.113	54.8
MCF7 xenograft_ Fasting+Tamoxifen_Replicate 3_PR	21069	0.044	40.5
MCF7 xenograft_control (no treatments)_INPUT	N.A	N.A	60.3
MCF7 xenograft_Tamoxifen treated_INPUT	N.A	N.A	38.7
MCF7 xenograft_ Fasting_INPUT	N.A	N.A	55.9
MCF7 xenograft_ Fasting + Tamoxifen_INPUT	N.A	N.A	62.3

Extended Data Table 2 | HR+BC patients treatment scheme from clinical trial NCT05748704

Patient number	TREATMENT
Pt 01	Decapeptil – Ribociclib + Letrozole
Pt 02	In the past Tamoxifen, now Etrozole + Decapeptyl
Pt 03	Enantone(q28) + Fulvestrant (q28) + Abemaciclib (everyday) Denosumab (q28)
Pt 04	Letrozole
Pt 05	Tamoxifen
Pt 06	Abemaciclib
Pt 07	Adjuvant chemotherapy Subsequently Adjuvant Radiotherapy Subsequently Aromatase Inhibitor
Pt 08	Exemestane + Decapeptyl
Pt 09	Exemestane + LHRH
Pt 10	Tamoxifen
Pt 11	Letrozole + Abemaciclib
Pt 12	Letrozole + Abemaciclib
Pt 13	Letrozole
Pt 14	Aromasin + Decapeptyl
Pt 15	Letrozole

Extended Data Table 3 | PR-activity gene signature

ABCC5	ECI2	LARP4	RASL10B
ABHD2	EFHD1	LEF1	RIF1
ADRB1	EGF	MAFB	RPS6KA1
ANKRD22	FAM105A	MAP3K3	SAP30
ARRB1	FAM46C	MAP4K5	SCD
ATF3	FAXDC2	MAPK1	SEC14L1
BBS10	FGF18	MON2	SGK1
BCAR1	FKBP5	NBPF10	SGK3
BCCIP	FOS	NEDD4	SHROOM3
BCL6	GADD45A	NEDD9	SLC45A1
BNIP3	GJB2	NFKBIA	SMPDL3B
C1orf116	GK	PAG1	SOS1
CCND1	GPR146	PAQR5	SREBF1
CDKN1C	GRB2	PARP9	TGFA
CDKN2AIP	HES2	PDK4	THBD
CEBPD	HMGB3	PISD	THBS1
CECR6	HMGCR	PLEKHF1	TMEM63C
CHST11	IL6ST	PLEKHF2	TP53BP2
CRY2	ITGA10	PLLP	UBE3A
CYB5B	JUN	PPL	UBR5
CYP51A1	KANSL1L	PPP1R14C	ZBED2
DHCR7	KAT2B	PRICKLE1	ZC3H12A
DNAAF2	KLF5	PRKAR2B	ZFP36
DUSP1	KLF6	PRR15	

nature portfolio

Corresponding author(s): Irene Caffa, Wilbert Zwart

Last updated by author(s): Oct 24, 2025

Reporting Summary

Nature Portfolio wishes to improve the reproducibility of the work that we publish. This form provides structure for consistency and transparency in reporting. For further information on Nature Portfolio policies, see our Editorial Policies and the Editorial Policy Checklist.

Statistics

For all statistical analyses, confirm that the following items are present in the figure legend, table legend, main text, or Methods section.

n/a	Confirmed
☐	☒ The exact sample size (*n*) for each experimental group/condition, given as a discrete number and unit of measurement
☐	☒ A statement on whether measurements were taken from distinct samples or whether the same sample was measured repeatedly
☐	☒ The statistical test(s) used AND whether they are one- or two-sided *Only common tests should be described solely by name; describe more complex techniques in the Methods section.*
☐	☒ A description of all covariates tested
☐	☒ A description of any assumptions or corrections, such as tests of normality and adjustment for multiple comparisons
☐	☒ A full description of the statistical parameters including central tendency (e.g. means) or other basic estimates (e.g. regression coefficient) AND variation (e.g. standard deviation) or associated estimates of uncertainty (e.g. confidence intervals)
☐	☒ For null hypothesis testing, the test statistic (e.g. *F*, *t*, *r*) with confidence intervals, effect sizes, degrees of freedom and *P* value noted *Give P values as exact values whenever suitable.*
☒	☐ For Bayesian analysis, information on the choice of priors and Markov chain Monte Carlo settings
☒	☐ For hierarchical and complex designs, identification of the appropriate level for tests and full reporting of outcomes
☐	☒ Estimates of effect sizes (e.g. Cohen's *d*, Pearson's *r*), indicating how they were calculated

Our web collection on statistics for biologists contains articles on many of the points above.

Software and code

Policy information about availability of computer code

Data collection	Band intensities of Western Blots were detected by Odyssey® CLx Imaging system (Li-Cor Biosciences) and ImageStudioTM Lite v.5.2.5 software (LI-COR Biosciences).
Data analysis	BWA 0.5.9-r26-dev, MACS2 (v2.1.2), DiffBind (v3.0.15), Rseb (v0.3.2) R-package (https://github.com/sebastian-gregoricchio/Rseb), ChIPseeker (v1.26.2), GIGGLE (http://dbtoolkit.cistrome.org/), deeptools (v2.5.3), bedtools (v2.25.0), HISAT2 (v2.1.0), DESeq2 (v1.30.1), clusterProfiler (v3.18.1), msigdbr (v7.5.1), ggplot2 (v3.3.5), ImageStudio™ Lite v.5.2.5.

For manuscripts utilizing custom algorithms or software that are central to the research but not yet described in published literature, software must be made available to editors and reviewers. We strongly encourage code deposition in a community repository (e.g. GitHub). See the Nature Portfolio guidelines for submitting code & software for further information.

Data

Policy information about availability of data

All manuscripts must include a data availability statement. This statement should provide the following information, where applicable:

- Accession codes, unique identifiers, or web links for publicly available datasets
- A description of any restrictions on data availability
- For clinical datasets or third party data, please ensure that the statement adheres to our policy

All mouse data generated or analysed during this study are included in this published article (and its supplementary information files). The in vitro data with human

cell lines are also available as Source Data. The ChIP-seq and RNA-seq data has been deposited to the GEO database (GSE260486). The mass spectrometry proteomics data have been deposited to the ProteomeXchange Consortium via the PRIDE49 partner repository with the dataset identifier PXD049477. BC patients' RNA-seq data are deposited on the European Genome-Phenome Archive (EGA) under accession number EGAS00001004944

Research involving human participants, their data, or biological material

Policy information about studies with human participants or human data. See also policy information about sex, gender (identity/presentation), and sexual orientation and race, ethnicity and racism.

Reporting on sex and gender	Blood samples and tissue samples from female breast cancer patients were used in this study.
Reporting on race, ethnicity, or other socially relevant groupings	Samples were derived from the IRCCS Ospedale Policlinico San Martino, in Genoa (NCT05748704) and the Fondazione IRCCS Istituto Nazionale dei Tumori, Milano (NCT03454282). Since samples have been pseudonymized, we do not have information about race/ethnicity.
Population characteristics	Female breast cancer patients. Race/ethnicity are not described in the study
Recruitment	IThe NCT05748704 trial was conducted at the IRCCS Ospedale Policlinico San Martino (Genoa), between December 2022 and February 2024 and was approved by the Comitato Etico Regione Liguria. This trial consists of a single-arm phase I/II clinical study of a FMD with solid tumours who are candidates to receive active medical or radiotherapy treatment (or with medical treatment or radiotherapy already ongoing). Inclusion Criteria were as follows: • Written informed consent • Age > 18 years • Patients with solid or hematologic tumors undergoing active treatment, including patients who are preparing to start a new treatment with chemotherapeutic regimens, hormone therapies, other molecularly targeted therapies (including kinase inhibitors), biologics (including trastuzumab) , pertuzumab, cetuximab and bevacizumab) or inhibitors of immune checkpoints (eg Opdivo, Keytruda), ie patients in whom treatment is already underway; • ECOG performance status 0-1 • Adequate organ function • BMI >21 kg/m2 (with possibility to also enroll patients with 19<BMI<21 based on the judgement of the treating physician) • Low nutritional risk according to nutritional risk screening (NRS) Exclusion criteria were as follows: • Age > 65 • Diabetes mellitus; • Previous therapy with IGF-1 inhibitors; • BMI <19 kg/m2; • bioimpedance phase angle <5.0°; • medium/high nutritional risk according to NRS; • Any metabolic disorder that can affect gluconeogenesis or ability to adapt to fasting periods; • Treatment in progress with other experimental therapies. All patients signed an informed consent for participating in the study, as well as for the use of clinical and biological data for research purposes. No bias that can impact on the results applies to this study. The DigesT study (NCT03454282) trial was conducted between July 2018 and December 2020 and in accordance with the Declaration of Helsinki and the principles of Good Clinical Practice. The study protocol was approved by the Institutional Review Board (IRB) and the Ethics Committee of Fondazione IRCCS Istituto Nazionale dei Tumori Milan, (INT 157/17). All patients provided written informed consent before any study procedures, as well as for the use of clinical and biological data for research purpose. Patients with resectable breast cancer (cT1N0M0 stage or cT1cN1M0-cT2cN0M0 stages not requiring pre-operative systemic treatment at the judgment of the investigator) who are candidate to curative surgery were enrolled; Were also enrolled patients with melanoma, that were not included in this study. Inclusion Criteria were as follows: • Age ≥ 18 and ≤ 75 years. • Evidence of a personally signed and dated informed consent document (ICD) indicating that the patient has been informed of all pertinent aspects of the study before enrollment and FMD prescription. • Willingness and ability to comply with the FMD protocol, the scheduled visits, treatment plans, laboratory tests and other procedures. • Histologically confirmed diagnosis of invasive breast cancer candidate to curative surgery. • For breast cancer patients, any biological subgroup (including estrogen receptor-positive, HER2-positive, triple-negative breast cancer) will be admitted; HER2-positive tumors will be defined on the basis of an IHC score of 3, or a score of 2 with ISH evaluation indicative of gene amplification. • Availability of archival FFPE tissue blocks of primary breast cancer. • Presence of an Eastern Cooperative Oncology Group (ECOG) performance status 0 or 1. • Presence of adequate bone marrow and organ function as defined by the following laboratory values: • ANC ≥ 1.5 x 109/l • platelets ≥ 100 x 109/l • hemoglobin ≥ 9.0 g/dl • calcium (corrected for serum albumin) within normal limits or ≤ grade 1 according to NCI-CTCAE version 4.03 if not clinically significant • potassium within the normal limits, or corrected with supplements • creatinine < 1.5 ULN

• blood uric acid < 10 mg/dl
• ALT and AST ≤ 2.5 x ULN
• total bilirubin < ULN except for patients with Gilbert syndrome who may only be included in the total bilirubin is < 3.0 x ULN or direct bilirubin < 1.5 x ULN
• Albumin > 3 g/dL
• Fasting glucose ≤ 200 mg/dl.
• Total Cholesterol ≤ 300 mg/dl.
• Triglycerides ≤ 300 mg/dl.

Female patients of childbearing potential must agree to sexual abstinence or to use two highly effective method of contraception throughout the study and for at least 30 days after the end of the FMD. Abstinence is only acceptable if it is in line with the preferred and usual lifestyle of the patient. Examples of contraceptive methods with a failure rate of < 1% per year include tubal ligation, male sterilization, hormonal implants, established, proper use of combined oral or injected hormonal contraceptives, and certain intrauterine devices. Alternatively, two methods (e.g., two barrier methods such as a condom and a cervical cap) may be combined to achieve a failure rate of < 1% per year. Barrier methods must always be supplemented with the use of a spermicide. A patient is of childbearing potential if, in the opinion of the Investigator, she is biologically capable of having children and is sexually active.

Female patients are not of childbearing potential if they meet at least one of the following criteria:
• Have undergone a documented hysterectomy and/or bilateral oophorectomy
• Have medically confirmed ovarian failure
• Achieved post-menopausal status, defined as: (≥ 12 months of non-therapy-induced amenorrhea) or surgically sterile (absence of ovaries) and have a serum FSH level within the laboratory's reference range for postmenopausal females.
Exclusion Criteria:
• Prior systemic treatment for breast cancer.
• Diagnosis of a concurrent malignancy other than breast cancer, or malignancy other than breast cancer diagnosed within 5 years of treatment enrollment, with the exception of adequately treated.
• Body Mass Index (BMI) < 20 Kg/m2.
• Anamnesis of alcohol abuse.
• Unintentional weight loss ≥ 5% in the last three months, unless the patient has a BMI > 25 Kg/m2 at study enrollment. Intentional weight loss is permitted if < 10% in the last three months and patient BMI is > 22 kg/m2.
• Severe heart, liver, pulmonary, kidney comorbidities.
• Current status of pregnancy or lactation, where pregnancy is defined as the state of a female after conception and until the termination of gestation, confirmed by a positive hCG laboratory test (> 5 mIU/mL).
• Active HBV or HCV infection.
• Severe infections within 4 weeks prior to FMD initiation, including, but not limited to, hospitalization for complications of infection, bacteremia, or severe pneumonia.
• Active autoimmune diseases that require systemic treatment (i.e. with use of disease modifying agents, corticosteroids or immunosuppressive drugs).
• History of recent diagnosis of hypothyroidism for which replacement therapy (eg., thyroxine) and blood endocrine profile are not stabilized yet.
• Established diagnosis of diabetes mellitus type I or diabetes mellitus type II that requires pharmacological treatment (including, but not limited to, insulin, insulin secretagogues and metformin).
• Severe impairment of the gastrointestinal (GI) function or GI disease that may alter the digestion and absorption of nutrients during the re-feeding phase (e.g. active ulcerative diseases of the stomach or intestine, uncontrolled nausea, vomiting, diarrhea, malabsorption syndrome, or small bowel resection).
• Known history of Human Immunodeficiency Virus (HIV) infection.
• Clinically significant heart disease and/or recent cardiac events including:
o history of angina pectoris, coronary artery bypass graft (CABG), symptomatic pericarditis, or myocardial infarction within 12 months prior to the start of study treatment;
o history of documented congestive heart failure (NYHA III-IV);
o documented cardiomyopathy.
• History of cardiac arythmias, (e.g. ventricular tachycardia, chronic atrial fibrillation), complete left bundle branch block, high grade AV block (e.g. bifascicular block, Mobitz type II and third degree AV block), supraventricular, nodal arrhythmias, or conduction abnormality in the previous 12 months.
• Uncontrolled hypertension defined by a Systolic Blood Pressure (SBP) ≥ 160 mmHg and/or Diastolic Blood Pressure (DBP) ≥ 100 mmHg, with or without anti-hypertensive medication.
• Known reduction of left-ventricular ejection fraction (LVEF) to less than 50%, as assessed by multigated radionuclide scintigraphic scan (MUGA) or echocardiography.
• Previous episodes of symptomatic hypotension causing unconsciousness.
• Baseline fasting plasma glucose ≤ 65 mg/dl.
• Ongoing therapy with systemic corticosteroids, or systemic corticosteroid therapy ≤ 2 weeks before study enrollment, or who have not recovered from side effects of such treatment. The following uses of corticosteroids are permitted: topical applications (e.g. for rash), inhaled sprays (e.g. for obstructive airways diseases), eye drops.
• Any serious medical or psychiatric illness that in the assessment of the investigator renders the patient not suitable for participation in this clinical study.

Ethics oversight

For the study NCT05748704, was approved by Comitato Etico Regione Liguria. For the study NCT03454282, was approved by the Institutional Review Board (IRB) and the Ethics Committee of Fondazione IRCCS Istituto Nazionale dei Tumori di Milano.

Note that full information on the approval of the study protocol must also be provided in the manuscript.

Field-specific reporting

Please select the one below that is the best fit for your research. If you are not sure, read the appropriate sections before making your selection.

☒ Life sciences ☐ Behavioural & social sciences ☐ Ecological, evolutionary & environmental sciences

For a reference copy of the document with all sections, see nature.com/documents/nr-reporting-summary-flat.pdf

Life sciences study design

All studies must disclose on these points even when the disclosure is negative.

Sample size	For our in vitro experiments, no statistical method was used to predetermine sample size, but our sample size were similar to those reported in several publication including ours (at least three technical replicates each experiment). For our in vivo experiments, we estimated sample size by PS (Power and Sample size calculation-Vanderbilt University) software considering a multifactorial variance analysis. By this approach we estimated that the minimum number of mice that was assigned to each treatment group in our in vivo experiments (typically n=5) would reach a power of 0.85. The Type I error probability associated with our tests of the null hypothesis was 0.05. For ChIP-seq and RNA-seq experiments , a minimal of n=3 was used for independent biological samples, to allow for t-test statistics. (doi: https://doi.org/10.1186/s13059-014-0550-8)
Data exclusions	No data were excluded
Replication	We confirm that all experiments were reproducible by repeating them several times and by using different lots of reagents, different stocks of cell lines and some experiments were also repeated and confirmed by other operators. All in vitro experiments were performed in, at least, 3 individual biological replicates, with at least 3 technical replicates per experiment. ChIP-seq, RNA-seq and proteomics were performed in, at least, 3 individual cell line or tumour samples. All IHC stainings were performed in, at least, 3 different tumour samples (except for GR staining of PDX 186). The immunofluorescence was performed 2 times, independently. The western blot was repeated 3 times, independently. In all cases, both individual and averaged results are shown.
Randomization	Samples and mice were assigned to the different experimental groups in a random fashion.
Blinding	Operators were unblinded with the exception of the pathologist who analyzed the samples from Fig. 2 and from Extended Data Fig. 1. Blinding during animal experiments was not possible because mice underwent a specific diet supply and daily treatment. Similarly, our clinical studies were one-arm studies and no blinding applied to these trials.

Reporting for specific materials, systems and methods

We require information from authors about some types of materials, experimental systems and methods used in many studies. Here, indicate whether each material, system or method listed is relevant to your study. If you are not sure if a list item applies to your research, read the appropriate section before selecting a response.

Materials & experimental systems

n/a	Involved in the study
☐	☒ Antibodies
☐	☒ Eukaryotic cell lines
☒	☐ Palaeontology and archaeology
☐	☒ Animals and other organisms
☐	☒ Clinical data
☒	☐ Dual use research of concern
☒	☐ Plants

Methods

n/a	Involved in the study
☐	☒ ChIP-seq
☐	☒ Flow cytometry
☒	☐ MRI-based neuroimaging

Antibodies

Antibodies used	ERα antibody (#06-935, Millipore, 5µg/IP) H3K27ac (#39133, Active Motif) --> https://www.activemotif.com/catalog/details/39133/histone-h3-acetyl-lys27-antibody-pab Glucocorticoid Receptor (GR, #12041S, Cell Signaling, 5µg/IP, 1:1000 for WB, 1:100 for IF) Progesterone Receptor (PR, #8757S, Cell Signaling, 5µg/IP) c-JUN (#9165S, Cell Signaling, 5µg/IP) β-actin (#MAB1501R, Millipore, 1:10000 for WB) Alexa Fluor™ 488 goat anti-rabbit IgG (#A-11008, ThermoFisher Scientific, 1:1000) Secondary antibodies donkey-α-mouse IRDye® 680RD (926-68073, LI-COR Biosciences, 1:10000) Secondary antibodies donkey-α-rabbit IRDye® 800CW (926-32213, LI-COR Biosciences, 1:10000) OmniMap anti-Rabbit HRP (760-4311, Ventana Medical systems)

KI-67 (5278384001, Ready-to-use, Roche Diagnostics/Ventana)
GR (for IHC, clone D6H2L, 1:600 dilution, 12041, Cell Signalling)
ERα (for IHC, clone SP1, Ready-to-use, 5278406001, Roche Diagnostics/Ventana)
PR (for IHC, clone 1E2 (Ready-to-Use, 527799001, Roche Diagnostics/Ventana)
Anti-Rabbit HQ (07017812001, Ventana Medical systems)
CD16/CD32 antibody (1:400, 553142, BD Bioscience)

Validation

ERα antibody (#06-935, Millipore) --> https://www.merckmillipore.com/NL/en/product/Anti-Estrogen-Receptor-Antibody,MM_NF-06-935. Tested in https://doi.org/10.1371/journal.pone.0215340
H3K27ac (#39133, Active Motif) --> https://www.activemotif.com/catalog/details/39133/histone-h3-acetyl-lys27-antibody-pab
Glucocorticoid Receptor (GR, #12041S, Cell Signaling) --> https://www.cellsignal.com/products/primary-antibodies/glucocorticoid-receptor-d6h2l-xp-rabbit-mab/12041
Progesterone Receptor (PR, #8757S, Cell Signaling) --> https://www.cellsignal.com/products/primary-antibodies/progesterone-receptor-a-b-d8q2j-xp-rabbit-mab/8757
c-JUN (#9165S, Cell Signaling) --> https://www.cellsignal.com/products/primary-antibodies/c-jun-60a8-rabbit-mab/9165
β-actin (#MAB1501R, Millipore) --> https://www.merckmillipore.com/NL/en/product/Anti-Actin-Antibodyclone-C4,MM_NF-MAB1501R
Alexa Fluor™ 488 goat anti-rabbit IgG (#A-11008, ThermoFisher Scientific) --> https://www.thermofisher.com/antibody/product/Goat-anti-Rabbit-IgG-H-L-Cross-Adsorbed-Secondary-Antibody-Polyclonal/A-11008
Secondary antibodies donkey-α-mouse IRDye® 680RD (926-68073, LI-COR Biosciences) --> https://www.licor.com/bio/reagents/irdye-680rd-donkey-anti-mouse-igg-secondary-antibody
Secondary antibodies donkey-α-rabbit IRDye® 800CW (926-32213, LI-COR Biosciences) --> https://www.licor.com/bio/reagents/irdye-800cw-donkey-anti-rabbit-igg-secondary-antibody
CD16/CD32 antibody (553142, BD Bioscience) --> https://www.bdbiosciences.com/en-pl/products/reagents/flow-cytometry-reagents/research-reagents/single-color-antibodies-ruo/purified-rat-anti-mouse-cd16-cd32-mouse-bd-fc-block.553142?tab=citations_references

Eukaryotic cell lines

Policy information about cell lines and Sex and Gender in Research

Cell line source(s)	The MCF7, T47D and HEK293T cell lines were purchased from the American Type Culture Collection (ATCC). TSAE1 cell line was a kind gift from Clare Isacke at ICR London.
Authentication	Authentication was performed by short tandem repeat profiling (Eurofins Genomics)
Mycoplasma contamination	Cell lines were subjected to regular Mycoplasma testing, by qPCR detection (MyTaq HS Red mix (bioline Bio-25047)) of 16S rRNA derived from several mycolplasma species.
Commonly misidentified lines (See ICLAC register)	None of the cell lines used in our study belongs to the Commonly misidentified lines.

Animals and other research organisms

Policy information about studies involving animals; ARRIVE guidelines recommended for reporting animal research, and Sex and Gender in Research

Laboratory animals	Six/eight-week-old female athymic nude mice (purchased from Envigo, Italy) were used in the experiments at the Animal Facility of the IRCCS Ospedale Policlinico San Martino (Genoa). 8-week-old female NSG mice (Jackson Laboratory) and BALB/c mice (Jackson Laboratory) were used in experiments performed at the Animal facility of the Netherlands Cancer Institute (NKI, Amsterdam).
Wild animals	The study did not involve wild animals.
Reporting on sex	All mice were female
Field-collected samples	The study did not involve field-collected samples.
Ethics oversight	Italian Istituto Superiore di Sanità and Organismo preposto al Benessere Animale (OPBA) of the IRCCS Ospedale Policlinico San Martino (Genoa, Italy) and Animal Ethics Committee of the Netherlands Cancer Institute.

Note that full information on the approval of the study protocol must also be provided in the manuscript.

Clinical data

Policy information about clinical studies

All manuscripts should comply with the ICMJE guidelines for publication of clinical research and a completed CONSORT checklist must be included with all submissions.

Clinical trial registration	Clinical trials NCT05748704 (IRCCS Ospedale Policlinico San Martino, Genoa, Italy) and NCT03454282 (Fondazione IRCCS Istituto Nazionale dei Tumouri, Milan, Italy).
Study protocol	Information on NCT05748704 trial can be obtained at: https://clinicaltrials.gov/ct2/show/NCT05748704. Information on NCT03454282 trial can be obtained at: https://clinicaltrials.gov/ct2/show/NCT03454282.

Data collection	In the NCT05748704 clinical trial, patients were enrolled and data were collected at the Department of Internal Medicine and Medical Specialties of the University of Genoa (Viale Benedetto XV 6, 16132 Genoa, Italy), Day Service, Room 1, between December 2022 and February 2024. In the NCT03454282 clinical trial, patients were enrolled and data were collected at the Fondazione IRCCS Istituto Nazionale dei Tumori, Milan, Onco-hematology Department, Medical Oncology 1 Unit, between July 2018 and December 2020.
Outcomes	In the NCT05748704 clinical trial, primary outcomes are the effects of the FMD regimen on the circulating levels of factors with pro- or anti-oncogenic activity (including insulin, IGF1, IGFBP1, IGFBP3, leptin, adiponectin, IL-6, TNF-alpha, IL1beta) as well as the effect of FMD cycles on leukocyte subpopulations with a role in tumor growth control, such as regulatory T cells, "myeloid-derived suppressor cells" (MDSCs) as well as NK cells, and its stem cell pool (e.g. e.g. hematopoietic stem cells, endothelial stem cells, mesenchymal stem cells). These biological parameters will be evaluated at the first, sixth and twelfth cycles of MF. Secondary outcomes are: - feasibility, measured as the percentage of prescribed diet consumed and intake of any extra food and monitored through the compilation of a food diary or via phone calls during the MF cycle - the effect of the MF on the microbioma composition. - clinical responses measured by CT, MRI or by blood chemistry tests, dosing of tumor markers and / or molecular biology tests in the case of prostate tumors or hematologic tumors (e.g. PSA in patients affected by prostate cancer, BCR / Abl mRNA in the case of patients undergoing treatment with kinase inhibitors for CML; CM in the case of patients undergoing treatment for multiple myeloma). -long-term efficacy (progression-free survival, overall survival). - effect of MF on circulating (blood) growth factors and adipokines, glucose, ketone bodies, and other metabolic parameters. In NCT03454282, the primary outcomes were the measuring of absolute and relative changes in PBMCs before and after the FMD. For the secondary outcomes, please consult https://clinicaltrials.gov/ct2/show/NCT03454282

Plants

Seed stocks	/
Novel plant genotypes	/
Authentication	/

ChIP-seq

Data deposition

☒ Confirm that both raw and final processed data have been deposited in a public database such as GEO.

☒ Confirm that you have deposited or provided access to graph files (e.g. BED files) for the called peaks.

Data access links *May remain private before publication.*	The ChIP-seq and RNA-seq data has been deposited to the GEO database (GSE260486, https://www.ncbi.nlm.nih.gov/geo/query/acc.cgi?acc=GSE260486).
Files in database submission	Paired-end fastq (*_R1/R2.fastq.gz) and bigWigs (*.bw): MCF7_Control_ER_Rep1 MCF7_Control_ER_Rep2 MCF7_Control_ER_Rep3 MCF7_TMX_ER_Rep1 MCF7_TMX_ER_Rep2 MCF7_TMX_ER_Rep3 MCF7_Fasting_ER_Rep1 MCF7_Fasting_ER_Rep2 MCF7_Fasting_ER_Rep3 MCF7_TMXplusFasting_ER_Rep1 MCF7_TMXplusFasting_ER_Rep2 MCF7_TMXplusFasting_ER_Rep3 MCF7_TMXplusFasting_ER_Rep4 MCF7_TMXplusFasting_ER_Rep5 MCF7_TMXplusFasting_ER_Rep6 MCF7_Control_H3K27ac_Rep1 MCF7_Control_H3K27ac_Rep2 MCF7_Control_H3K27ac_Rep3 MCF7_TMX_H3K27ac_Rep1 MCF7_TMX_H3K27ac_Rep2 MCF7_TMX_H3K27ac_Rep3

MCF7_Fasting_H3K27ac_Rep1
MCF7_Fasting_H3K27ac_Rep2
MCF7_Fasting_H3K27ac_Rep3
MCF7_TMXplusFasting_H3K27ac_Rep1
MCF7_TMXplusFasting_H3K27ac_Rep2
MCF7_TMXplusFasting_H3K27ac_Rep3
MCF7_TMXplusFasting_H3K27ac_Rep4
MCF7_TMXplusFasting_H3K27ac_Rep5
MCF7_TMXplusFasting_H3K27ac_Rep6
MCF7_Control_GR_Rep1
MCF7_Control_GR_Rep2
MCF7_Control_GR_Rep3
MCF7_TMX_GR_Rep1
MCF7_TMX_GR_Rep2
MCF7_TMX_GR_Rep3
MCF7_Fasting_GR_Rep1
MCF7_Fasting_GR_Rep2
MCF7_Fasting_GR_Rep3
MCF7_TMXplusFasting_GR_Rep1
MCF7_TMXplusFasting_GR_Rep2
MCF7_TMXplusFasting_GR_Rep3
MCF7_Control_cJUN_Rep1
MCF7_Control_cJUN_Rep2
MCF7_Control_cJUN_Rep3
MCF7_TMX_cJUN_Rep1
MCF7_TMX_cJUN_Rep2
MCF7_TMX_cJUN_Rep3
MCF7_Fasting_cJUN_Rep1
MCF7_Fasting_cJUN_Rep2
MCF7_Fasting_cJUN_Rep3
MCF7_TMXplusFasting_cJUN_Rep1
MCF7_TMXplusFasting_cJUN_Rep2
MCF7_TMXplusFasting_cJUN_Rep3
MCF7_Control_PR_Rep1
MCF7_Control_PR_Rep2
MCF7_Control_PR_Rep3
MCF7_TMX_PR_Rep1
MCF7_TMX_PR_Rep2
MCF7_TMX_PR_Rep3
MCF7_Fasting_PR_Rep1
MCF7_Fasting_PR_Rep2
MCF7_Fasting_PR_Rep3
MCF7_TMXplusFasting_PR_Rep1
MCF7_TMXplusFasting_PR_Rep2
MCF7_TMXplusFasting_PR_Rep3
MCF7_Control_INPUT
MCF7_TMX_INPUT
MCF7_Fasting_INPUT
MCF7_TMXplusFasting_INPUT

Bed files (peaks):
MCF7_Control_ER_Rep1_chr.narrowPeak
MCF7_Control_ER_Rep2_chr.narrowPeak
MCF7_Control_ER_Rep3_chr.narrowPeak
MCF7_TMX_ER_Rep1_chr.narrowPeak
MCF7_TMX_ER_Rep2_chr.narrowPeak
MCF7_TMX_ER_Rep3_chr.narrowPeak
MCF7_Fasting_ER_Rep1_chr.narrowPeak
MCF7_Fasting_ER_Rep2_chr.narrowPeak
MCF7_Fasting_ER_Rep3_chr.narrowPeak
MCF7_TMXplusFasting_ER_Rep1_chr.narrowPeak
MCF7_TMXplusFasting_ER_Rep2_chr.narrowPeak
MCF7_TMXplusFasting_ER_Rep3_chr.narrowPeak
MCF7_TMXplusFasting_ER_Rep4_chr.narrowPeak
MCF7_TMXplusFasting_ER_Rep5_chr.narrowPeak
MCF7_TMXplusFasting_ER_Rep6_chr.narrowPeak
MCF7_Control_H3K27ac_Rep1_chr.narrowPeak
MCF7_Control_H3K27ac_Rep2_chr.narrowPeak
MCF7_Control_H3K27ac_Rep3_chr.narrowPeak
MCF7_TMX_H3K27ac_Rep1_chr.narrowPeak
MCF7_TMX_H3K27ac_Rep2_chr.narrowPeak
MCF7_TMX_H3K27ac_Rep3_chr.narrowPeak
MCF7_Fasting_H3K27ac_Rep1_chr.narrowPeak
MCF7_Fasting_H3K27ac_Rep2_chr.narrowPeak
MCF7_Fasting_H3K27ac_Rep3_chr.narrowPeak
MCF7_TMXplusFasting_H3K27ac_Rep1_chr.narrowPeak

MCF7_TMXplusFasting_H3K27ac_Rep2_chr.narrowPeak
MCF7_TMXplusFasting_H3K27ac_Rep3_chr.narrowPeak
MCF7_TMXplusFasting_H3K27ac_Rep4_chr.narrowPeak
MCF7_TMXplusFasting_H3K27ac_Rep5_chr.narrowPeak
MCF7_TMXplusFasting_H3K27ac_Rep6_chr.narrowPeak
MCF7_Control_GR_Rep1_chr.narrowPeak
MCF7_Control_GR_Rep2_chr.narrowPeak
MCF7_Control_GR_Rep3_chr.narrowPeak
MCF7_TMX_GR_Rep1_chr.narrowPeak
MCF7_TMX_GR_Rep2_chr.narrowPeak
MCF7_TMX_GR_Rep3_chr.narrowPeak
MCF7_Fasting_GR_Rep1_chr.narrowPeak
MCF7_Fasting_GR_Rep2_chr.narrowPeak
MCF7_Fasting_GR_Rep3_chr.narrowPeak
MCF7_TMXplusFasting_GR_Rep1_chr.narrowPeak
MCF7_TMXplusFasting_GR_Rep2_chr.narrowPeak
MCF7_TMXplusFasting_GR_Rep3_chr.narrowPeak
MCF7_Control_cJUN_Rep1_chr.narrowPeak
MCF7_Control_cJUN_Rep2_chr.narrowPeak
MCF7_Control_cJUN_Rep3_chr.narrowPeak
MCF7_TMX_cJUN_Rep1_chr.narrowPeak
MCF7_TMX_cJUN_Rep2_chr.narrowPeak
MCF7_TMX_cJUN_Rep3_chr.narrowPeak
MCF7_Fasting_cJUN_Rep1_chr.narrowPeak
MCF7_Fasting_cJUN_Rep2_chr.narrowPeak
MCF7_Fasting_cJUN_Rep3_chr.narrowPeak
MCF7_TMXplusFasting_cJUN_Rep1_chr.narrowPeak
MCF7_TMXplusFasting_cJUN_Rep2_chr.narrowPeak
MCF7_TMXplusFasting_cJUN_Rep3_chr.narrowPeak
MCF7_Control_PR_Rep1_chr.narrowPeak
MCF7_Control_PR_Rep2_chr.narrowPeak
MCF7_Control_PR_Rep3_chr.narrowPeak
MCF7_TMX_PR_Rep1_chr.narrowPeak
MCF7_TMX_PR_Rep2_chr.narrowPeak
MCF7_TMX_PR_Rep3_chr.narrowPeak
MCF7_Fasting_PR_Rep1_chr.narrowPeak
MCF7_Fasting_PR_Rep2_chr.narrowPeak
MCF7_Fasting_PR_Rep3_chr.narrowPeak
MCF7_TMXplusFasting_PR_Rep1_chr.narrowPeak
MCF7_TMXplusFasting_PR_Rep2_chr.narrowPeak
MCF7_TMXplusFasting_PR_Rep3_chr.narrowPeak

Genome browser session
(e.g. UCSC)

Genomics and transcriptomics data access details:
- GSE260486 (https://www.ncbi.nlm.nih.gov/geo/query/acc.cgi?acc=GSE260486)

Methodology

Replicates

For each condition, a minimum of 3 samples were sequenced

Sequencing depth

All the samples were paired-end sequenced

sample n_peaks FRiP M_reads_mapped
MCF7 xenograft_control (no treatments)_Replicate 1_ER 29741 0.078 61.5
MCF7 xenograft_control (no treatments)_Replicate 2_ER 33150 0.095 49.7
MCF7 xenograft_control (no treatments)_Replicate 3_ER 13670 0.039 55.6
MCF7 xenograft_Tamoxifen treated_Replicate 1_ER 47243 0.138 62.3
MCF7 xenograft_Tamoxifen treated_Replicate 2_ER 9365 0.022 58.1
MCF7 xenograft_Tamoxifen treated_Replicate 3_ER 34206 0.098 53.1
MCF7 xenograft_ Fasting_Replicate 1_ER 46901 0.147 56.0
MCF7 xenograft_ Fasting_Replicate 2_ER 47993 0.148 76.2
MCF7 xenograft_ Fasting_Replicate 3_ER 37040 0.102 70.4
MCF7 xenograft_ Fasting + Tamoxifen_Replicate 1_ER 72054 0.257 67.0
MCF7 xenograft_ Fasting + Tamoxifen_Replicate 2_ER 49417 0.156 61.8
MCF7 xenograft_ Fasting + Tamoxifen_Replicate 3_ER 61939 0.203 64.2
MCF7 xenograft_ Fasting + Tamoxifen_Replicate 4_ER 40273 0.147 48.8
MCF7 xenograft_ Fasting + Tamoxifen_Replicate 5_ER 711 0.003 38.2
MCF7 xenograft_ Fasting + Tamoxifen_Replicate 6_ER 25818 0.087 35.0
MCF7 xenograft_control (no treatments)_Replicate 1_H3K27ac 57810 0.538 43.2
MCF7 xenograft_control (no treatments)_Replicate 2_H3K27ac 49081 0.636 51.7
MCF7 xenograft_control (no treatments)_Replicate 3_H3K27ac 57808 0.604 66.2
MCF7 xenograft_Tamoxifen treated_Replicate 1_H3K27ac 53674 0.675 68.2
MCF7 xenograft_Tamoxifen treated_Replicate 2_H3K27ac 63146 0.562 59.7
MCF7 xenograft_Tamoxifen treated_Replicate 3_H3K27ac 61864 0.588 70.1
MCF7 xenograft_ Fasting_Replicate 1_H3K27ac 60350 0.568 55.1

MCF7 xenograft_ Fasting_Replicate 2_H3K27ac 62978 0.571 67.8
MCF7 xenograft_ Fasting_Replicate 3_H3K27ac 59070 0.538 52.7
MCF7 xenograft_ Fasting + Tamoxifen_Replicate 1_H3K27ac 52298 0.634 59.9
MCF7 xenograft_ Fasting + Tamoxifen_Replicate 2_H3K27ac 57696 0.579 58.9
MCF7 xenograft_ Fasting + Tamoxifen_Replicate 3_H3K27ac 54060 0.587 67.9
MCF7 xenograft_ Fasting + Tamoxifen_Replicate 4_H3K27ac 62138 0.594 61.1
MCF7 xenograft_ Fasting + Tamoxifen_Replicate 5_H3K27ac 69495 0.414 49.8
MCF7 xenograft_ Fasting + Tamoxifen_Replicate 6_H3K27ac 63469 0.498 55.5
MCF7 xenograft_control (no treatments)_Replicate 1_GR 6514 0.007 35.6
MCF7 xenograft_control (no treatments)_Replicate 2_GR 5452 0.015 34
MCF7 xenograft_control (no treatments)_Replicate 3_GR 357 0.051 42.8
MCF7 xenograft_Tamoxifen treated_Replicate 1_GR 820 0.003 37.9
MCF7 xenograft_Tamoxifen treated_Replicate 2_GR 3944 0.007 36.8
MCF7 xenograft_Tamoxifen treated_Replicate 3_GR 1312 0.002 24.7
MCF7 xenograft_ Fasting_Replicate 1_GR 16421 0.039 46.7
MCF7 xenograft_ Fasting_Replicate 2_GR 22725 0.059 39.1
MCF7 xenograft_ Fasting_Replicate 3_GR 21758 0.053 51.8
MCF7 xenograft_ Fasting + Tamoxifen_Replicate 1_GR 9669 0.02 29.9
MCF7 xenograft_ Fasting + Tamoxifen_Replicate 2_GR 33000 0.099 41.1
MCF7 xenograft_ Fasting + Tamoxifen_Replicate 3_GR 2447 0.005 34
MCF7 xenograft_control (no treatments)_Replicate 1_c-JUN 44567 0.078 23.9
MCF7 xenograft_control (no treatments)_Replicate 2_c-JUN 44402 0.135 34.3
MCF7 xenograft_control (no treatments)_Replicate 3_c-JUN 12203 0.087 36.2
MCF7 xenograft_Tamoxifen treated_Replicate 1_c-JUN 9248 0.017 34.5
MCF7 xenograft_Tamoxifen treated_Replicate 2_c-JUN 42874 0.145 30.7
MCF7 xenograft_Tamoxifen treated_Replicate 3_c-JUN 49230 0.088 24.5
MCF7 xenograft_ Fasting_Replicate 1_c-JUN 28022 0.087 39.1
MCF7 xenograft_ Fasting_Replicate 2_c-JUN 36738 0.131 36.6
MCF7 xenograft_ Fasting_Replicate 3_c-JUN 30904 0.096 22.4
MCF7 xenograft_ Fasting + Tamoxifen_Replicate 1_c-JUN 32444 0.067 20.1
MCF7 xenograft_ Fasting + Tamoxifen_Replicate 2_c-JUN 50206 0.208 36.3
MCF7 xenograft_ Fasting + Tamoxifen_Replicate 3_c-JUN 33115 0.084 33.6
MCF7 xenograft_control (no treatments)_Replicate 1_PR 10825 0.019 35.1
MCF7 xenograft_control (no treatments)_Replicate 2_PR 21080 0.043 37.2
MCF7 xenograft_control (no treatments)_Replicate 3_PR 14426 0.033 43.6
MCF7 xenograft_Tamoxifen treated_Replicate 1_PR 5939 0.011 31.7
MCF7 xenograft_Tamoxifen treated_Replicate 2_PR 27179 0.056 38.8
MCF7 xenograft_Tamoxifen treated_Replicate 3_PR 4298 0.008 27.9
MCF7 xenograft_ Fasting_Replicate 1_PR 26274 0.055 53.3
MCF7 xenograft_ Fasting_Replicate 2_PR 39145 0.083 52.7
MCF7 xenograft_ Fasting_Replicate 3_PR 29032 0.068 44.9
MCF7 xenograft_ Fasting + Tamoxifen_Replicate 1_PR 21180 0.06 23.9
MCF7 xenograft_ Fasting + Tamoxifen_Replicate 2_PR 50226 0.113 54.8
MCF7 xenograft_ Fasting + Tamoxifen_Replicate 3_PR 21069 0.044 40.5
MCF7 xenograft_control (no treatments)_INPUT N.A N.A 60.3
MCF7 xenograft_Tamoxifen treated_INPUT N.A N.A 38.7
MCF7 xenograft_ Fasting_INPUT N.A N.A 55.9
MCF7 xenograft_ Fasting + Tamoxifen_INPUT N.A N.A 62.3

Antibodies

ERα antibody (#06-935, Millipore, 5µg/IP)
H3K27ac (#39133, Active Motif, 5µg/IP)
Glucocorticoid Receptor (GR, #12041S, Cell Signaling, 5µg/IP)
Progesterone Receptor (PR, #8757S, Cell Signaling, 5µg/IP)
c-JUN (#9165S, Cell Signaling, 5µg/IP)

Peak calling parameters

MAPPING:
bwa mem -M -t {threads} -p hg38 sample_R1.fastq.gz 2> | samtools view -Sbu - | samtools sort -m 2G -T sample -@ {threads} -O bam - > sample.bam

PEAK calling
macs2 callpeak -t target.bam -c input.bam -f BAM -g 2861343702 -q 0.01 --outdir outdir --name sample_peaks

Data quality

Reads were filtered based on mapping quality (MAPQ ≥ 20), and duplicate reads were marked with Picard MarkDuplicates (v2.19.0). MACS2 (v2.1.2) was used to perform peak calling over input ChIP-seq samples; only peaks with a q-value < 0.01 were retained.

Software

Reads were aligned to the human genome build GRCh38 using BWA 0.5.9-r26-dev. Reads with a mapping quality (MAPQ) < 20 were removed from further analysis. Enrichment over input control was determined using MACS2. Only peaks not overlapping with the ENCODE Hg38/GRCh38 blacklisted regions, were retained.

Flow Cytometry

Plots

Confirm that:

☒ The axis labels state the marker and fluorochrome used (e.g. CD4-FITC).

☒ The axis scales are clearly visible. Include numbers along axes only for bottom left plot of group (a 'group' is an analysis of identical markers).

☒ All plots are contour plots with outliers or pseudocolor plots.

☒ A numerical value for number of cells or percentage (with statistics) is provided.

Methodology

Sample preparation	BC nodules were macrodissected from TSAE1-bearing mice and processed to generate single-cell suspensions using the Tumour Dissociation Kit (Miltenyi Biotec, cat.no. 130-096-730) in conjunction with the gentleMACS Octo Dissociator, following the manufacturers' protocols. The cell pellet of in vivo samples were incubated with anti-CD16/CD32 antibody (BD Bioscience) and stained with the antibodies against surface markers following standard procedures. Samples were fixed with the eBioscience fixation and permeabilization kit (Invitrogen), and stained for intracellular markers.
Instrument	Samples were acquired using a five-laser Aurora spectral flow cytometer (Cytek Biosciences)
Software	FlowJo v10 software.
Cell population abundance	Not applicable as no sorts were performed.
Gating strategy	To determine the populations of myeloid and lymphoid cells, we first used SSC, FSC and Zombie-NIR (live/dead dye) gating to select for single cell and live cell events. Immune cell populations were then identified by their high expression levels of CD45. The following populations were then identified from the immune cell compartment: lymphoid cells (CD45+ CD11b-). Myeloid cells (CD45+ CD11b+). From myeloid cells, we gated neutrophils (CD45+ CD11b+ Ly6G+), non-classical monocytes (CD45+ CD11b+ Ly6G- Ly6C-) and dendritic cells (CD45+ F4/80- CD11chigh MHCIIhigh).

☒ Tick this box to confirm that a figure exemplifying the gating strategy is provided in the Supplementary Information.